New Phytologist

An extracellular β-*N*-acetylhexosaminidase of *Medicago truncatula* hydrolyzes chitooligosaccharides and is involved in arbuscular mycorrhizal symbiosis but not required for nodulation

Yi-Han Wang[1], Wei Liu[1], Jing Cheng[1], Ru-Jie Li[1], Jiangqi Wen[2], Kirankumar S. Mysore[2], Zhi-Ping Xie[1], Didier Reinhardt[3] and Christian Staehelin[1]

[1]State Key Laboratory of Biocontrol and Guangdong Key Laboratory of Plant Resources, School of Life Sciences, Sun Yat-sen University, Guangzhou 510275, China; [2]Institute for Agricultural Biosciences, Oklahoma State University, Ardmore, OK 73401, USA; [3]Department of Biology, University of Fribourg, 1700 Fribourg, Switzerland

Authors for correspondence:
Christian Staehelin
Email: cst@mail.sysu.edu.cn

Didier Reinhardt
Email: didier.reinhardt@unifr.ch

Received: *27 February 2023*
Accepted: *18 May 2023*

New Phytologist (2023) **239:** 1954–1973
doi: 10.1111/nph.19094

Key words: arbuscular mycorrhizal symbiosis, chitooligosaccharides, glycoside hydrolase, *Medicago truncatula*, *N*-acetylglucosamine, β-*N*-acetylhexosaminidase.

Summary

- Establishment of symbiosis between plants and arbuscular mycorrhizal (AM) fungi depends on fungal chitooligosaccharides (COs) and lipo-chitooligosaccharides (LCOs). The latter are also produced by nitrogen-fixing rhizobia to induce nodules on leguminous roots. However, host enzymes regulating structure and levels of these signals remain largely unknown.
- Here, we analyzed the expression of a β-*N*-acetylhexosaminidase gene of *Medicago truncatula* (*MtHEXO2*) and biochemically characterized the enzyme. Mutant analysis was performed to study the role of *MtHEXO2* during symbiosis.
- We found that expression of *MtHEXO2* is associated with AM symbiosis and nodulation. *MtHEXO2* expression in the rhizodermis was upregulated in response to applied chitotetraose, chitoheptaose, and LCOs. *M. truncatula* mutants deficient in symbiotic signaling did not show induction of *MtHEXO2*. Subcellular localization analysis indicated that MtHEXO2 is an extracellular protein. Biochemical analysis showed that recombinant MtHEXO2 does not cleave LCOs but can degrade COs into *N*-acetylglucosamine (GlcNAc). *Hexo2* mutants exhibited reduced colonization by AM fungi; however, nodulation was not affected in *hexo2* mutants.
- In conclusion, we identified an enzyme, which inactivates COs and promotes the AM symbiosis. We hypothesize that GlcNAc produced by MtHEXO2 may function as a secondary symbiotic signal.

Introduction

Molecular communication is at the center of all symbiotic interactions of plants with microbes. Particularly well understood are the symbiosis with arbuscular mycorrhizal (AM) fungi and the interaction between legumes and nodule bacteria collectively referred to as rhizobia. In roots colonized by AM fungi, host plants can benefit from enhanced access to mineral nutrients in the soil, especially phosphorus. In the nodule symbiosis, legumes obtain fixed nitrogen from rhizobia which are able to reduce atmospheric nitrogen into ammonia (Perret *et al.*, 2000; Smith & Read, 2008; Wang *et al.*, 2022; Yang *et al.*, 2022).

At the molecular level, symbiotic signaling in both symbioses shows overlaps. The ease of genetic analysis in bacteria allowed the identification of lipo-chitooligosaccharides (LCOs) as rhizobial signals required for nodule formation. Subsequently, components of nodulation signaling in legumes such as *Medicago truncatula* have been identified (Roy *et al.*, 2020; Yang *et al.*, 2022). Rhizobial LCOs, also known as Nod factors, consist of an oligomeric ($n = 3$–6) *N*-acetylglucosamine (GlcNAc) backbone with an acyl group at the nonreducing end. LCOs produced by different rhizobial strains are structurally diverse and often decorated by reducing end modifications such as a sulfate group (Perret *et al.*, 2000). The interaction between LCOs and LCO receptors in legumes can result in host-specific nodulation, that is, nodules of a given legume are only formed with specific rhizobial strains (Radutoiu *et al.*, 2007; Walker *et al.*, 2020).

Interestingly, LCOs are also produced by AM fungi (Maillet *et al.*, 2011) and by various nonsymbiotic fungi (Rush *et al.*, 2020). In addition, nonmodified chitooligosaccharides (COs; $n = 4$–8), secreted or released from fungal chitin (poly-GlcNAc) by endochitinases of fungal or plant origin, can trigger characteristic symbiotic responses in host plants (Feng *et al.*, 2019; Khokhani *et al.*, 2021; Crosino & Genre, 2022; Volpe *et al.*, 2023). For example, nuclear calcium oscillations, known as calcium spiking, are essential features of symbiotic signaling induced by rhizobial LCOs (Ehrhardt *et al.*, 1996) and mycorrhizal COs/LCOs (Genre *et al.*, 2013; Sun *et al.*, 2015). Chitin and COs are also signals for pathogen recognition because they indicate the presence of fungi with chitinous cell walls. Clear

evidence for an overlap between recognition of AM fungi and fungal pathogens is the involvement of a shared receptor component, the lysin-motif-type (LysM) receptor CERK1 (Khokhani *et al.*, 2021; Zhang *et al.*, 2021; Crosino & Genre, 2022).

To trigger symbiotic signaling in host plants, rhizobial LCOs and COs/LCOs of AM fungi are perceived by ligand-induced heterodimerization of two different LysM receptors (Gibelin-Viala *et al.*, 2019; Girardin *et al.*, 2019; He *et al.*, 2019; Bozsoki *et al.*, 2020; Roy *et al.*, 2020; Zhang *et al.*, 2021). Downstream of these receptors, a shared signaling pathway (common symbiosis signaling pathway; CSSP), relays the signal from the plasma membrane to the nucleus, where calcium spiking and a calcium- and calmodulin-dependent protein kinase (CCaMK; named DMI3 in *M. truncatula*) control a transcriptional cascade to activate hundreds of symbiotic genes (Genre & Russo, 2016; Roy *et al.*, 2020).

Plant chitinases (glycoside hydrolase families 18 and 19) not only hydrolyze chitin and COs (Drula *et al.*, 2022) but also may have the capacity to degrade and inactivate LCOs (Staehelin *et al.*, 1994a,b; Goormachtig *et al.*, 1998; Schultze *et al.*, 1998; Ovtsyna *et al.*, 2000; Tian *et al.*, 2013; Cai *et al.*, 2018; Li *et al.*, 2022). Mutant analysis revealed a symbiotic role of the LCO-cleaving family 18 glycoside hydrolases MtNFH1/MtCHIT5b in *M. truncatula* and LjCHIT5 in *Lotus japonicus*, indicating that concentration and distribution of rhizobial LCOs are under precise control during nodulation (Cai *et al.*, 2018; Malolepszy *et al.*, 2018; Li *et al.*, 2022). COs/LCOs of AM fungi are believed to be inactivated by host enzymes to maintain optimal signal concentration and to avoid chitin-triggered induction of defense responses. Fungal chitinases (Khokhani *et al.*, 2021; Crosino & Genre, 2022) and host chitinases such as MtCHIT 3-3 of *M. truncatula* (Elfstrand *et al.*, 2005) are thought to hydrolyze chitin and COs of AM fungi.

In addition to chitinases, enzymes of the glycoside hydrolase family 20 (GH20) can cleave COs. Most GH20 enzymes are exotype enzymes that remove terminal nonreducing GlcNAc or *N*-acetylgalactosamine (GalNAc) residues from oligosaccharides or glycoconjugates such as *N*-glycans of *N*-glycosylated proteins. GH20 enzymes with such β-*N*-acetylhexosaminidase activity are produced by various organisms, including rhizobia, AM fungi, and plants (Liu *et al.*, 2018; Drula *et al.*, 2022). In *Arabidopsis thaliana*, three GH20 enzymes (AtHEXO1, AtHEXO2, and AtHEXO3) have been characterized with respect to their enzymatic properties and subcellular localization. Vacuolar AtHEXO1 and apoplastic AtHEXO3 were found to show high activity on pyridylaminated *N*-glycans, while plasmalemma-resident AtHEXO2 preferentially cleaved pyridylaminated chitotriose (Gutternigg *et al.*, 2007; Strasser *et al.*, 2007; Liebminger *et al.*, 2011; Castilho *et al.*, 2014). More recently, related GH20 enzymes of *Nicotiana benthamiana* with different substrate preference for *N*-glycans including two plasmalemma-resident NbHEXO2 isoforms have been characterized (Alvisi *et al.*, 2021).

Here, we asked whether a GH20 enzyme in *M. truncatula* cleaves COs and plays a role in AM symbiosis. We found that rhizodermal expression of the *MEDICAGO TRUNCATULA β-N-ACETYLHEXOSAMINIDASE* 2 (*MtHEXO2*) gene is upregulated in response to applied COs and LCOs. MtHEXO2 fused to red fluorescent protein (RFP) or green fluorescent protein (GFP) was detected in the rhizodermis of roots inoculated with AM fungi or rhizobia. Recombinant MtHEXO2 protein could efficiently hydrolyze COs. *M. truncatula* mutants with a *Tnt1* retrotransposon insertion in *MtHEXO2* showed reduced colonization by AM fungi, but were not impaired in nodulation.

Materials and Methods

Biological materials

Escherichia coli DH5α was used for plasmid construction. Recombinant protein expression was performed with *E. coli* BL21(DE3) and *Pichia pastoris* (Guillierm.) Phaff GS115. *Sinorhizobium* (*Ensifer*) *meliloti* Rm41 and a derivative constitutively expressing the red fluorescent protein mCherry were used for inoculation experiments. LCOs were purified from *S. meliloti* 1021 (pEK327) (Schultze *et al.*, 1992) and *Sinorhizobium* sp. NGR234. NGRΔ*nodABC* deficient in LCO synthesis (Price *et al.*, 1992) served as a control. *Agrobacterium tumefaciens* EHA105 (Hood *et al.*, 1993) was used for stable transformation and *A. rhizogenes* LBA9402 (Hooykaas & Hooykaas, 2021) for hairy root transformation. The AM fungus *Rhizophagus intraradices* (Schenk & Sm.) Walker & Schüßler BGC BJ09 was obtained from BGC (Bank of Glomales in China, Beijing, China) and multiplied using *Sorghum bicolor* (L.) Moench plants. Isolation of *Fusarium oxysporum* Schlechtendal (emend. Snyder & Hansen) F06 has been described previously (Liu *et al.*, 2012).

The *M. truncatula* Gaertner ecotypes Jemalong A17 and R108 were used in this study. The nodulation signaling mutants *dmi3-1* and *dmi1-3* of Jemalong A17 (mutants Y6 and TRV25; Sagan *et al.*, 1998; Catoira *et al.*, 2000) were kindly provided by Clare Gough (INRAE-CNRS, Castanet-Tolosan, France). The mutant lines *hexo2-1* (NF4082) and *hexo2-2* (NF5709) of the R108 ecotype carrying a *Tnt1* retrotransposon insertion in *MtHEXO2* were obtained from the *Medicago Tnt1* mutant collection currently hosted by the Institute of Agricultural Biosciences, Oklahoma State University, Ardmore, USA (Tadege *et al.*, 2008; Pislariu *et al.*, 2012).

Gene cloning, plasmids, and primers

Details on plasmids and primers used in this study are shown in Supporting Information Tables S1, S2. Plant genomic DNA was purified with the HP Plant DNA Kit from Omega Bio-tek (Norcross, GA, USA). All constructs were verified by sequencing.

To clone the coding sequence of *MtHEXO2* (*Medtr2g062560* in Mt4.0; *MtrunA17Chr2g0309231* in Mt5.0), the two exon sequences amplified from genomic DNA of *M. truncatula* (ecotypes R108 and Jemalong A17) were assembled by overlap extension PCR.

For protein expression, the coding sequence of *MtHEXO2* (without the 18-amino signal peptide predicted by SignalP-6.0) was inserted into pET-28a (for *E. coli*) and pPIC9K (for *P. pastoris*). To obtain an enzymatically inactive MtHEXO2 variant, nucleotides encoding the predicted catalytic residues (D325 and

E326) were mutated by overlap extension PCR and cloned into pET-28a. For antibody production, pET-MtHEXO2(119–463), a pET-28a derivative containing DNA encoding a truncated version of MtHEXO2 (residues 119 to 463), was constructed.

For experiments with *MtHEXO2* promoter–reporter gene constructs, 2630-bp (Jemalong A17) and 2628-bp (R108) promoter sequences were cloned from *M. truncatula* genomic DNA and fused to a β-glucuronidase (*GUS*) reporter gene sequence (with an intron derived from pCAMBIA1305.1). The obtained $MtHEXO2_{pro}$-*GUS* constructs were cloned into pBluescript II KS (−). In parallel, a derivative of the binary vector pCAMBIA1302 with DNA encoding RFP was constructed by replacing the *mGFP5* sequence with an *RFP* expression cassette derived from pX-DR (Chen *et al.*, 2009) using *Bgl*II and *Pml*I (plasmid pCAMBIA1302-*RFP*). Finally, the $MtHEXO2_{pro}$-*GUS* constructs were inserted into pCAMBIA1302-*RFP* using *Kpn*I and *Hind*III.

To explore subcellular localization of MtHEXO2 in *M. truncatula* roots, hairy root transformation was performed with a pCAMBIA1302 derivative that contained the native 2628-bp promoter sequence of R108 and the coding sequence with a C-terminal *RFP* tag. A control plasmid was constructed by cloning a promoterless *RFP* fragment from pX-DR into pCAMBIA1302 digested with *BamH*I and *Spe*I (excision of the CaMV 35S promoter). A similar strategy was used for the construction of a vector containing the 2628-bp promoter sequence and a *MtHEXO2:GFP* fusion construct.

To restore the wild-type (WT) phenotype in inoculation experiments with AM fungi, hairy roots of *hexo2* mutants expressing *MtHEXO2* were analyzed. DNA consisting of $MtHEXO2_{pro}$, the *MtHEXO2* coding sequence, and a poly(A) tail was inserted into pCAMBIA1302-*RFP* digested with *Kpn*I and *Hind*III. The plasmid pCAMBIA1302-*RFP* served as a control.

To create *MtHEXO2*-overexpressing *M. truncatula* plants, the coding sequence of *MtHEXO2* (ecotype Jemalong A17) was cloned as a *BamH*I-*Xho*I fragment into the binary vector pISV2678 carrying a double cauliflower mosaic virus (CaMV) 35S promoter (constructed by Michael Schultze, CNRS, Gif-sur-Yvette, France). The obtained plasmid pISV-*MtHEXO2* was then mobilized into *A. tumefaciens* EHA105.

Expression of MtHEXO2 in *E. coli* and *P. pastoris*

For expression of His-tagged MtHEXO2 in *E. coli*, the plasmids pET-28a, pET-MtHEXO2, and pET-MtHEXO2(DE) were transformed into competent BL21(DE3) cells. Cultures containing 0.5 mM isopropyl-β-D-thiogalactopyranoside were shaken at 18°C for 20 h. Harvested bacteria were sonicated, and His-tagged MtHEXO2 was purified using Ni-NTA resin beads and an elution buffer (pH 8.0) containing 50 mM NaH_2PO_4, 300 mM NaCl and 250 mM imidazole. Details are described in Methods S1. MtHEXO2 protein was also obtained from culture supernatants of *P. pastoris* GS115 transformants obtained by electro-transformation with pPIC9K-*MtHEXO2* linearized with *Sad*I. The plasmid pPIC9K alone served as a control. Transformation and protein expression procedures were performed according to the *Pichia* Expression System Manual (Invitrogen). Protein expression was induced by 0.5% methanol, and cultures were harvested at different time points. Culture supernatants containing secreted MtHEXO2 protein were obtained by centrifugation. Details on MtHEXO2 expression in *P. pastoris* can be found in Methods S2.

Protein analysis and Western blots

Protein analysis on SDS-PAGE was performed according to standard procedures. Western blot analysis was performed either with a commercially available anti-His antibody (TransGen Biotech, Beijing, China) or with a rabbit antiserum raised against a truncated form of MtHEXO2 (residues 119–463) expressed in *E. coli* BL21(DE3). Further information can be found in Methods S3.

LCOs, COs, and sulfated chitobiose

The tetrameric LCO NodSm-IV(C16:2, S) was purified from *S. meliloti* 1021 (pEK327) as described previously (Schultze *et al.*, 1992; Staehelin *et al.*, 1994b; Tian *et al.*, 2013) with the exception that the *n*-butanol extraction procedure was replaced by the use of Amberlite XAD-2 beads (Sigma-Aldrich), which were directly added to the bacterial culture supernatant ($40\ g\ l^{-1}$). LCOs bound to the beads were eluted with 40 ml methanol and 30 ml acetone. Purification of NodSm-IV(C16:2, S) by high-pressure liquid chromatography (HPLC) was performed as reported previously (Staehelin *et al.*, 1994b). Furthermore, LCOs of *Sinorhizobium* sp. NGR234 (Price *et al.*, 1992), which are structurally similar to fungal LCOs (Rush *et al.*, 2020), were obtained from bacterial culture supernatants. In parallel, control material was obtained from the mutant strain NGRΔ*nodABC*, which is unable to produce LCOs (Price *et al.*, 1992). LCO synthesis was induced by 1 μM apigenin. Harvested culture supernatants were mixed with Amberlite XAD-2 beads, and bound LCOs were eluted with methanol and acetone. The eluates were dried with a rotary evaporator and then dissolved in water containing 20% DMSO. Yields of LCOs were estimated by quantification of reducing end sugars (Lever, 1972). Further details are provided in Methods S4.

COs were purchased from Seikagaku Kogyo Co. (Tokyo, Japan) or Elicityl (Grenoble, France). Sulfated chitobiose was prepared by complete hydrolysis of NodSm-IV(C16:2, S) with recombinant MtNFH1 (Tian *et al.*, 2013). After incubation, the lipo-disaccharide NodSm-II(C16:2) was removed by extraction with *n*-butanol and the aqueous phase containing sulfated chitobiose was dried in a speed-vac evaporator. Further information on the procedure can be found in Methods S5.

Medicago truncatula plants were treated with COs, NodSm-IV (C16:2, S), or LCOs of *Sinorhizobium* sp. NGR234 in Jensen medium (Van Brussel *et al.*, 1982). Where indicated, the solution contained DMSO at a final concentration of 0.5% (v/v). Further details are given in Methods S6.

Enzyme assays

Activity of recombinant MtHEXO2 was determined using different *p*-nitrophenyl (*p*NP) glycosides (Sigma-Aldrich) at a

concentration of 1 mM. The reaction mixture was incubated at 37°C for 1 h. Hydrolysis of aryl glycosides results in the production of *p*-nitrophenol, which can be photometrically detected at 405 nm. Further information on the experimental conditions can be found in Methods S7.

Activity of recombinant MtHEXO2 toward COs (1 mM) was determined by photometrically measuring the produced GlcNAc with *p*-dimethylaminobenzaldehyde (DMAB) according to Reissig *et al.* (1955). The samples were incubated at 37°C for 1.5 h. Further details are given in Methods S8.

Hydrolysis of chitopentaose by MtHEXO2 expressed in *P. pastoris* was also analyzed by reverse-phase HPLC using an amino column (μBondapak NH2 column 0.8 × 10 cm; Waters, Milford, MA, USA) according to Tian *et al.* (2013). Further information on the procedure can be found in Methods S9.

Thin-layer chromatography (TLC) was used to analyze whether sulfated chitobiose is resistant to hydrolysis by MtHEXO2 expressed in *P. pastoris*. Samples were separated on Silica gel 60 F254 plates (Merck) using ethyl acetate : acetic acid : water (3 : 2 : 1 v/v/v) as mobile phase. Sugars were visualized with a diphenylamine-aniline-phosphoric acid reagent. Additional details can be found in Methods S10.

HPLC was used to analyze NodSm-IV(C16:2, S) and the cleavage product NodSm-II(C16:2) after incubation with chitinase from *Streptomyces griseus* (Sigma-Aldrich). A parallel test was performed with NodSm-IV(C16:2, S) and recombinant MtHEXO2 from *P. pastoris*. Further details can be found in Methods S11. Similar enzyme tests were performed with LCOs from *Sinorhizobium* sp. NGR234, and reducing end sugars were photometrically determined with the Lever assay (Methods S12).

Seed germination, growth conditions, and plant inoculation

Medicago truncatula seeds were surface-sterilized with diluted commercial bleach. Details are described in Methods S13. Plants were kept in a growth room at 24°C and a 16-h photoperiod as described previously (Cai *et al.*, 2018).

Medicago truncatula plants were inoculated with AM fungi and harvested at different time points. The inoculum containing small root fragments was prepared by co-cultivating *R. intraradices* BGC BJ09 with sorghum plants. For inoculation of *M. truncatula*, sterilized plastic jar units linked with a cotton wick were used. Mock inoculation was performed with sterilized substrate without fungus. Details are provided in Methods S14. Furthermore, surface-sterilized *R. intraradices* spores (Chabaud *et al.*, 2006b) were locally applied to roots grown on agar plates containing modified Fahraeus medium (Boisson-Dernier *et al.*, 2001). A similar spot inoculation experiment was also carried out with a mycelium of *F. oxysporum* F06 (Liu *et al.*, 2012).

Inoculation of *M. truncatula* with *S. meliloti* was conducted in 300-ml plastic jar units containing vermiculite and expanded clay (3 : 1 v/v) in the upper jar (1 plant per jar unit). Details on the inoculation procedure can be found in Methods S15.

Root colonization by AM fungi

Roots were washed with water and then immersed in 10% (w/v) KOH at 95°C for 10–15 min. After washing with water for several times, roots were transferred to an ink-vinegar solution (ratio 1 : 19; v/v) at 95°C for 3 min (Vierheilig *et al.*, 1998). After removing the staining solution, roots were repeatedly rinsed with 5% acetic acid. Roots were microscopically observed with a stereo microscope (Lumar.V12; Zeiss). The degree of root colonization by AM fungi and the frequency of different AM structures (hyphopodia, internal hyphae, arbuscules, and vesicles) were determined with a gridline intersection method (Giovannetti & Mosse, 1980). Where indicated, AM structures of GUS-stained roots were visualized by WGA-AF488 (wheat germ agglutinin conjugated to Alexa Fluor 488 obtained from Thermo Fisher Scientific) using a Zeiss Axio Imager Z1 fluorescence microscope. Details of the procedure are given in Methods S16.

Protein localization analysis

Hairy roots of *M. truncatula* expressing *MtHEXO2:RFP* or transformed with a control plasmid were inoculated with *R. intraradices*. Plants were harvested at 8–10 d post inoculation (dpi) and analyzed by a confocal laser scanning microscope following the instructions of the user manual (Leica TCS SP5; Leica, Wetzlar, Germany).

In addition, hairy roots of *M. truncatula* expressing *MtHEXO2:GFP* or transformed with a control plasmid were inoculated with *S. meliloti* Rm41 expressing mCherry. Roots were harvested at 2–3 dpi, and root hairs with infection pockets were analyzed by a Zeiss Axio Imager Z1 fluorescence microscope. Further information on microscopic protein localization analysis is provided in Methods S17.

Plant transformation

Hairy root transformation of *M. truncatula* plants was achieved according to previously described protocols (Boisson-Dernier *et al.*, 2001; Chabaud *et al.*, 2006a). The tip of radicles was cut off, and the wounded area of the seedling was immersed into a prepared bacterial lawn (*A. rhizogenes* LBA9402 carrying a given binary vector). Seedlings were transferred onto 0.9% (w/v) agar plates containing nitrogen-free Fahraeus medium (Fahraeus, 1957). After 6 d, small hairy roots emerging from the formed callus were removed and seedlings were transferred onto 0.9% (w/v) agar plates containing modified Fahraeus medium (Boisson-Dernier *et al.*, 2001). Further information on the transformation procedure is given in Methods S18.

In addition, *A. tumefaciens* EHA105 carrying pISV-*MtHEXO2* was used to create stable *M. truncatula* R108 transformants constitutively expressing *MtHEXO2* under the control of a tandem CaMV 35S promoter. The transformation procedure was performed according to previously published protocols (Hoffmann *et al.*, 1997; Trinh *et al.*, 1998). Briefly, leaf disks of 6-wk-old plants were infiltrated with a suspension of agrobacteria. The explants were cultivated on SHMab and SHM2 plates

supplemented with 500 mg l^{-1} cefotaxime and 6 mg l^{-1} Basta. Induction of shoot formation was performed with SHM2 plates without cefotaxime and Basta. ½SHM2 plates were used to induce root formation. Plants with elevated *MtHEXO2* transcripts were used for seed propagation and subsequent experiments. Further details are given in Methods S19.

Histochemical GUS staining and sectioning of nodules

Hairy roots and nodules transformed with the *MtHEXO2*$_{pro}$-*GUS* construct were subjected to histochemical GUS staining using 5-bromo-4-chloro-3-indol-β-glucuronic acid (X-Gluc). Paraffin-embedded nodules were sectioned and microscopically analyzed. Further information on these procedures is provided in Methods S20.

qRT-PCR analysis

Quantitative real-time PCR (qRT-PCR) was used to analyze transcript levels of *M. truncatula* genes. RNA was extracted from roots with the RNAprep pure Plant Kit (Tiangen Biotech, Beijing, China) and converted into cDNA by reverse transcription using HiScript II Q RT SuperMix (Vazyme, Nanjing, China). Each PCR reaction (10 µl) contained 1 µl cDNA template (10 ng), 0.25 µM of each primer (Table S2), and 5 µl of the LightCycler 480 SYBR Green I Master reaction mix (Roche). The thermocycling conditions using a LightCycler 480 PCR instrument (Roche) were set as follows: (1) preincubation: 95°C for 5 min; (2) amplification (45 cycles): 95°C for 30 s, 58°C for 30 s, and 72°C for 20 s; (3) melting curve analysis: 95°C for 5 s and 65°C for 1 min; (4) cooling: 40°C for 10 min. PCRs with each cDNA were performed in triplicate. *Ubiquitin* (*Medtr5g076340*) served as a housekeeping gene. Roche LightCycler 480 software was used to calculate the threshold cycles (C_t values). Where indicated, *MtHEXO2* expression analysis was also performed by reverse transcription PCR using agarose gels for amplicon analysis.

Bioinformatic tools

Gene sequences were retrieved from the NCBI homepage (https://www.ncbi.nlm.nih.gov) and the *Medicago truncatula* Hapmap Project homepage (http://www.medicagohapmap.org/) using the Basic Local Alignment Search Tool (Blast). Sequence alignments were conducted with Megalign software (https://www.dnastar.com/). Primers were designed with the help of the Oligo 7 software (http://www.oligo.net/index.html). The Promoter 2.0 Prediction Server (http://www.cbs.dtu.dk/services/promoter/) was used for promoter prediction. Signal peptide prediction was performed with SignalP-6.0 (https://services.healthtech.dtu.dk/services/SignalP-6.0/). Information on gene expression was downloaded from the *Medicago truncatula* Gene Expression Atlas (MtExpress V3) web server (https://medicago.toulouse.inrae.fr/MtExpress) and the Symbimics database (https://iant.toulouse.inra.fr/symbimics), respectively. For phylogenetic analysis, sequence alignments were conducted with Mega11 software by using the ClustalW method and the phylogenetic tree was constructed using the neighbor-joining method (https://www.megasoftware.net/).

Results

The *M. truncatula* genome contains three β-*N*-acetylhexosaminidase genes

Gene chip hybridization and RNA sequencing studies on *M. truncatula* indicated an increased expression of the β-*N*-acetylhexosaminidase gene *Medtr2g062560* in roots inoculated with AM fungi (Gomez *et al.*, 2009; Gaude *et al.*, 2012; Afkhami & Stinchcombe, 2016; Luginbuehl *et al.*, 2017; Zeng *et al.*, 2018; Fernández *et al.*, 2019), while inoculation with *S. meliloti* showed minor effects on gene expression (Benedito *et al.*, 2008; Breakspear *et al.*, 2014; Liu *et al.*, 2019; Schiessl *et al.*, 2019). Fig. S1 provides corresponding information from the *M. truncatula* Gene Expression Atlas (Carrere *et al.*, 2021). RNA sequencing experiments also revealed that WT roots treated with COs show slightly elevated *Medtr2g062560* expression compared with CO-treated mutant lines impaired in CO perception (Feng *et al.*, 2019). A treatment of roots with COs over weeks had no or little impact on *Medtr2g062560* expression in mycorrhizal and nonmycorrhizal roots (Volpe *et al.*, 2023). On the contrary, a rapid induction of *Medtr2g062560* expression was observed in rhizodermal cells when roots were treated with LCOs from *S. meliloti* (Jardinaud *et al.*, 2016; Fig. S2), while no significant effects of LCOs on *Medtr2g062560* expression were observed in another study (Damiani *et al.*, 2016).

Medtr2g062560 encodes a GH20 enzyme with a canonical motif in the core of the catalytic site (HXGXDE motif in GH20 enzymes; X stands for any amino acid). Asp^{325} (D) and Glu^{326} (E) of Medtr2g062560 are predicted catalytic residues required for enzyme activity (Hou *et al.*, 2001; Gutternigg *et al.*, 2007; Strasser *et al.*, 2007; Liu *et al.*, 2018; Fig. S3).

A Blast search at the *M. truncatula* Hapmap project homepage with *Medtr2g062560* as a query sequence yielded two homologous genes (*Medtr1g115475* and *Medtr7g023060*). A protein sequence alignment indicated that the predicted Medtr1g115475 and Medtr7g023060 proteins are related to AtHEXO1 of *A. thaliana* (amino acid identity 68% and 72%, respectively), while Medtr2g062560 is likely orthologous to AtHEXO2 of *A. thaliana* (amino acid identity 64%; Fig. S3). We therefore named the *MtHEXO* (*Medicago truncatula* β-*N*-acetylhexosaminidase) genes as follows: *MtHEXO1a* (*Medtr1g115475*), *MtHEXO1b* (*Medtr7g023060*), and *MtHEXO2* (*Medtr2g062560*). The canonical HXGXDE motif was found to be conserved in all three predicted MtHEXO proteins (Fig. S3). In contrast to *MtHEXO2*, transcript levels of *MtHEXO1a* and *MtHEXO1b* do not appear to be increased during AM symbiosis (Gomez *et al.*, 2009; Gaude *et al.*, 2012; Afkhami & Stinchcombe, 2016; Luginbuehl *et al.*, 2017; Zeng *et al.*, 2018; Fernández *et al.*, 2019; Carrere *et al.*, 2021; Fig. S1).

Phylogenetic analysis suggests that *MtHEXO1a* and *MtHEXO1b* evolved through gene duplication. Members of the *HEXO2* clade were found in genomes of various mono- and

dicotyledonous plants, most of which are capable of establishing an AM symbiosis (Fig. S4). RNA sequencing data indicate that, compared with nonmycorrhizal roots, the expression of *HEXO2* homologs is elevated in mycorrhizal roots in various plants, including tomato (Solyc01g081610; Tominaga *et al.*, 2022; Zeng *et al.*, 2023) and rice (LOC_Os07g38790; Fiorilli *et al.*, 2015; Gutjahr *et al.*, 2015). The *HEXO3* clade appears to lack leguminous genes (Fig. S4). Analysis of exon–intron structures confirmed that *MtHEXO1a* and *MtHEXO1b* are related to *AtHEXO1* while *MtHEXO2* is most similar to *AtHEXO2* (Fig. S5).

MtHEXO2 expression is upregulated during symbiosis

To explore the *MtHEXO2* expression pattern during symbiosis, a 2628-bp promoter sequence of *MtHEXO2* was cloned from *M. truncatula* R108 and fused to the *GUS* reporter gene to yield $MtHEXO2_{pro}$-*GUS*. The binary vector also contained an *RFP* expression cassette under the control of a constitutive promoter. Plants with transformed hairy roots showing red fluorescence were inoculated with *R. intraradices* and harvested at different time points. *MtHEXO2* promoter activity was then visualized by GUS staining. *MtHEXO2* promoter activity was visible in the central cylinder independently of inoculation with AM fungi under these test conditions. In contrast to control plants, rhizodermal cells of inoculated plants showed clear blue coloration at early but not later time points (Fig. 1a). An induction of *MtHEXO2* promoter activity was also observed for rhizodermal (or cortical) cells when surface-sterilized spores of *R. intraradices* were applied locally to roots of plants grown on plates while no or only faint blue coloration of the central cylinder was observed

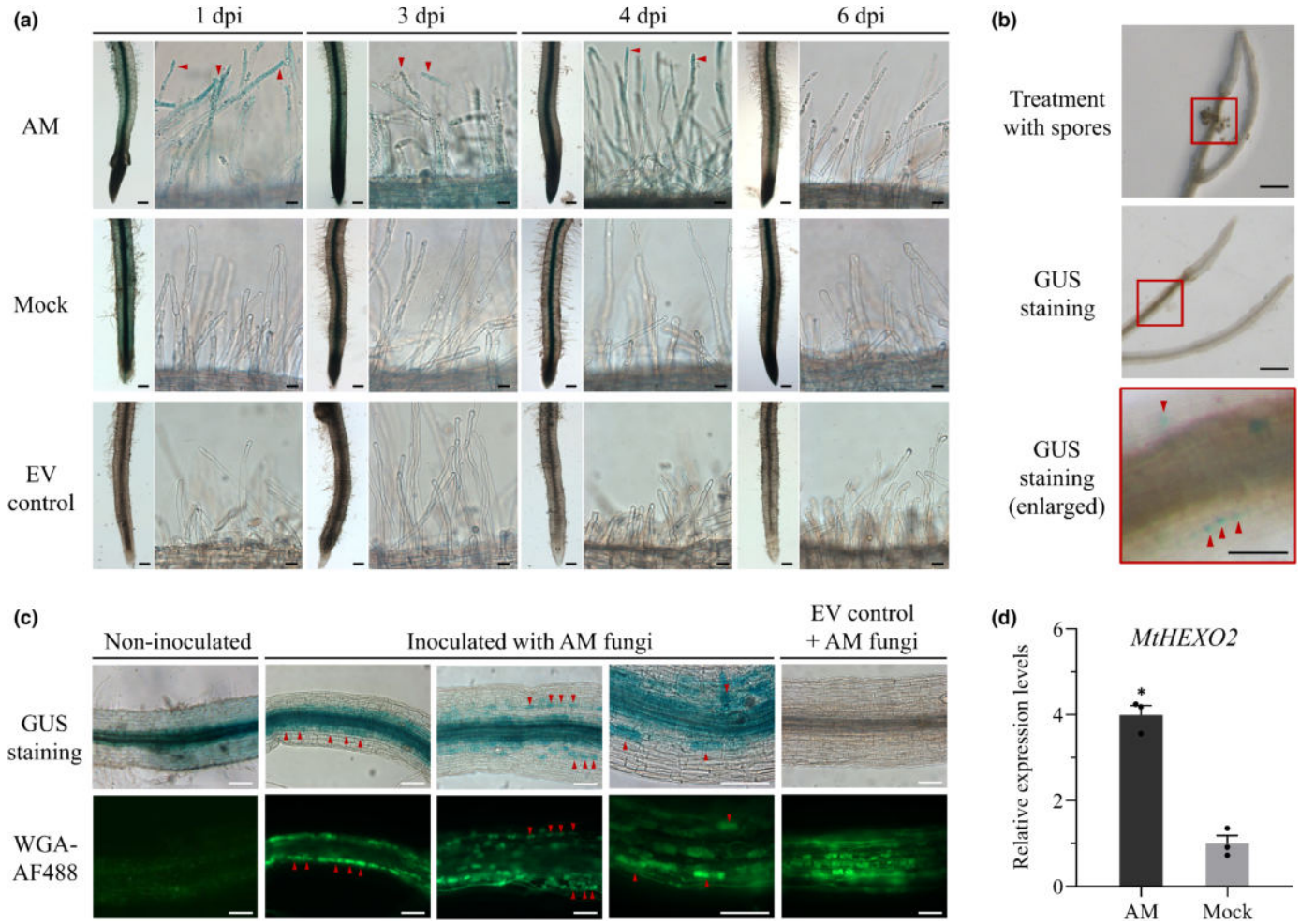

Fig. 1 Analysis of *MtHEXO2* expression in mycorrhizal *Medicago truncatula* R108 roots. (a) GUS staining in roots expressing $MtHEXO2_{pro}$-*GUS* (or empty vector) and inoculated with *Rhizophagus intraradices* (arbuscular mycorrhizal (AM)) or sterilized substrate (Mock). Pictures show representative examples of whole roots (bars, 200 μm) and rhizodermal cells (bars, 20 μm) from 5 to 8 biological replicates. Arrowheads mark blue root hairs. (b) Induction of $MtHEXO2_{pro}$-*GUS* after local inoculation with *R. intraradices* spores (red frame) for 24 h. Pictures show the same root before and after GUS staining (bars, 500 μm). The enlarged picture corresponds to the red-bordered area (bar, 100 μm). Arrowheads indicate blue-colored cells after GUS staining. (c) Correlation of mycorrhizal structures and $MtHEXO2_{pro}$-*GUS* expression in roots inoculated with *R. intraradices* (40 d post inoculation (dpi)). Roots were subjected to GUS staining and then treated with WGA-AF488 (green fluorescent signals). Arrowheads indicate arbuscules. Noninoculated roots and inoculated roots transformed with the empty vector (EV) served as controls (bars, 100 μm). (d) qRT-PCR analysis of *MtHEXO2* in wild-type (WT) plants inoculated with *R. intraradices* (30 dpi). RNA samples represent roots of three pooled plants. Data indicate means ± SE of normalized expression values ($n = 3$). The asterisk indicates a significant increase of *MtHEXO2* transcripts in mycorrhizal roots (two-tailed Student's *t*-test: *, *P*-value ≤ 0.01).

under these plant growth conditions (Fig. 1b). By contrast, spot inoculation by the fungal pathogen *F. oxysporum* did not lead to induction of *MtHEXO2* promoter activity at the treatment site (Fig. S6). To analyze roots colonized by AM fungi, plants were harvested at 40 dpi and then subjected to GUS staining followed by incubation with WGA-AF488 to visualize fungal structures by fluorescence microscopy. Blue coloration reflecting *MtHEXO2* promoter activity was observed in the central cylinder of mycorrhizal and nonmycorrhizal roots. However, colonization by AM fungi resulted in increased blue coloration in the root cortex, particularly in arbuscule-containing cells. Arbuscules showing strong fluorescence were often but not always stained blue, suggesting that *MtHEXO2* expression was transiently stimulated in these cells (Fig. 1c). In another experiment, expression of *MtHEXO2* was analyzed by qRT-PCR in mycorrhizal and nonmycorrhizal roots at 30 dpi. The result confirmed that *MtHEXO2* expression was upregulated in mycorrhizal roots (Fig. 1d).

To explore *MtHEXO2* expression during early stages of the nodule symbiosis, hairy roots transformed with the $MtHEXO2_{pro}$-*GUS* construct were inoculated with *S. meliloti* Rm41 and harvested at different time points. Root tissue (cortex and central cylinder) of inoculated as well as mock-inoculated plants occasionally showed faint blue coloration, indicating constitutive *MtHEXO2* expression in the examined roots. However, *MtHEXO2* promoter activity was clearly induced in young root hairs at 1 dpi while root hairs of mock-inoculated plants were not blue. Later time points showed weak or no blue coloration in root hairs of inoculated plants, indicating transient induction of *MtHEXO2* expression upon rhizobial inoculation (Fig. 2a).

Nodules harvested at 10 dpi or 20 dpi showed blue coloration that merged into the blue-colored central cylinder of the root. Photographs of paraffin sections indicated that highest *MtHEXO2* expression in nodules was associated with vascular bundles (Fig. 2b).

MtHEXO2 expression in the rhizodermis is upregulated by symbiotic signals

COs from AM fungi are known symbiotic signals for *M. truncatula* (Genre *et al.*, 2013; Feng *et al.*, 2019). We therefore applied chitotetraose and chitoheptaose to hairy roots of R108 plants transformed with the $MtHEXO2_{pro}$-*GUS* construct. Roots treated for 4 h with these COs showed GUS activity in the rhizodermis, particularly in young root hairs close to the root tip. However, no blue coloration of rhizodermal cells was observed when roots were analyzed 24 h after the CO treatment. Neither mock-treated control plants, nor plants transformed with the empty vector and treated with COs, showed blue coloration of rhizodermal cells at any time point. Similar to the treatment with COs, the LCO NodSm-IV(C16:2, S) of the symbiont *S. meliloti* induced *MtHEXO2* promoter activity in root hairs close to the root tip at 4-h postapplication, but not at 24 h (Fig. 3a). Furthermore, we examined the effects of LCOs from *Sinorhizobium* sp. NGR234, which does not nodulate *M. truncatula* (Pueppke & Broughton, 1999). This strain produces many types of LCOs that are structurally similar to fungal LCOs including those from *R. intraradices* (Price *et al.*, 1992; Rush *et al.*, 2020). Interestingly, LCOs from NGR234 were able to induce *MtHEXO2* promoter activity in rhizodermal *M. truncatula* cells expressing $MtHEXO2_{pro}$-*GUS*. Blue root hair cells were observed at 4 h after LCO application, but not at 24 h. Roots treated with the control material obtained from NGRΔ*nodABC* (deficient in LCO synthesis) remained colorless (Fig. 3b).

MtHEXO2 expression in the rhizodermis requires a functional CSSP

To further characterize the observed effects of COs and LCOs on *MtHEXO2* expression, experiments were performed with *dmi3-1*

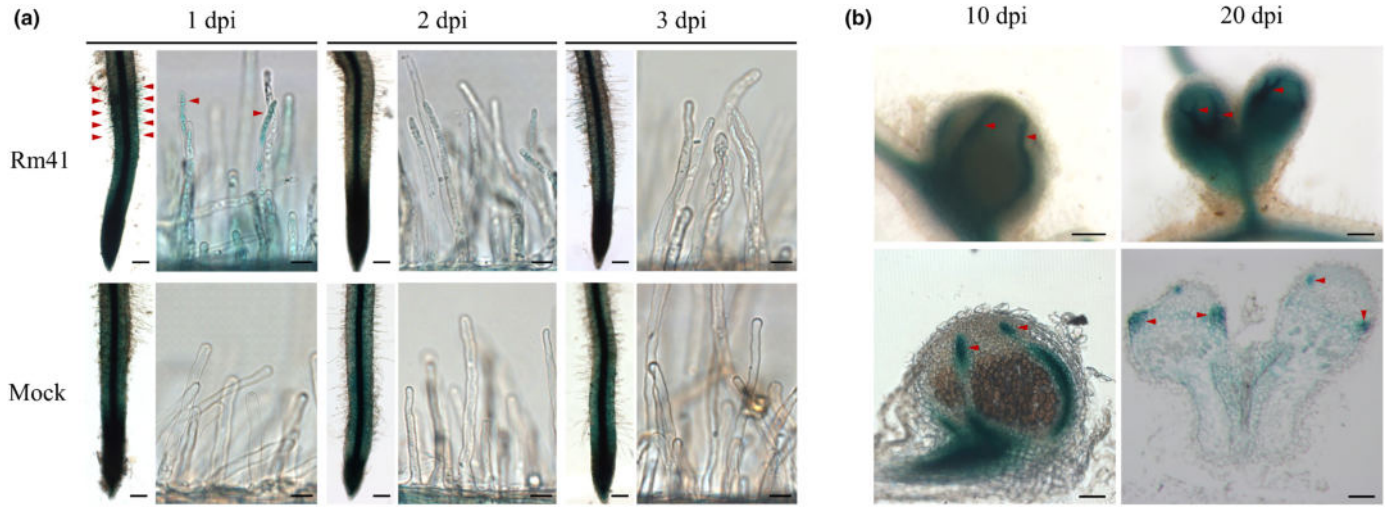

Fig. 2 Analysis of *Medicago truncatula* R108 roots transformed with $MtHEXO2_{pro}$-*GUS* and inoculated with rhizobia. (a) Transformed roots were inoculated with *Sinorhizobium meliloti* Rm41 or mock-treated with 10 mM $MgSO_4$. Pictures show whole roots (bars, 200 μm) and root hairs (bars, 20 μm) at the time of harvest. Arrowheads mark blue root hairs in the infection zone close to the root tip. (b) Pictures of GUS-stained nodules harvested at indicated time points (upper; bars, 200 μm) and corresponding paraffin sections (lower; bars, 100 μm). Arrowheads mark vascular bundles.

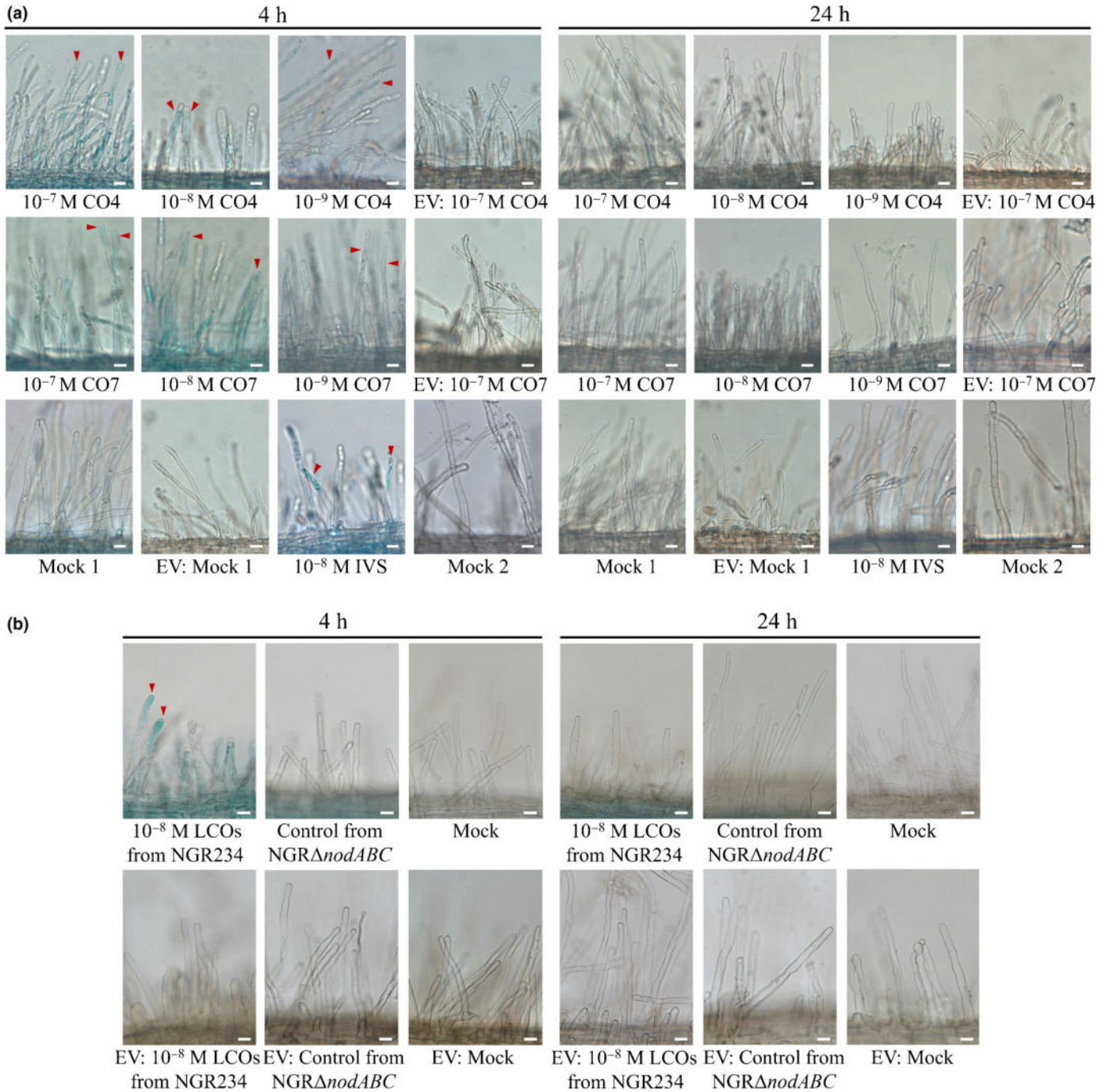

Fig. 3 GUS activity in rhizodermal cells of *Medicago truncatula* R108 roots transformed with *MtHEXO2*$_{pro}$-*GUS* and treated with COs, NodSm-IV(C16:2, S) or LCOs from NGR234 for 4 h or 24 h. Plants transformed with the empty vector (EV) were also analyzed. (a) Transformed roots were treated with indicated concentrations of chitotetraose (CO4) or chitoheptaose (CO7) dissolved in Jensen medium or with 10^{-8} M NodSm-IV(C16:2, S) dissolved in Jensen medium containing 0.5% (v/v) DMSO (abbreviated as 10^{-8} IVS). Control plants were treated with Jensen medium (Mock 1) or Jensen medium containing 0.5% (v/v) DMSO (Mock 2). (b) Transformed roots were treated with 10^{-8} M LCOs from NGR234 dissolved in Jensen medium containing 0.5% (v/v) DMSO. A control treatment was performed with corresponding material from the NGRΔ*nodABC* mutant. Control plants were treated with Jensen medium containing 0.5% (v/v) DMSO (Mock). Arrowheads mark blue coloration of young root hairs close to the root tip. Bars, 20 μm.

and *dmi1-3*, mutants of *M. truncatula* Jemalong A17 which are unable to induce CSSP-mediated gene expression because of a defect in CCaMK and a nuclear cation channel, respectively (Lévy *et al.*, 2004; Mitra *et al.*, 2004; Capoen *et al.*, 2011). As the promoter sequence of Jemalong A17 is slightly different from R108 plants (nucleotide identity 90%; Fig. S7), we cloned a *MtHEXO2* 2630-bp promoter sequence from Jemalong A17 and constructed a corresponding binary vector with the *GUS* reporter

gene. Hairy roots of WT plants expressing *MtHEXO2*$_{pro}$*-GUS* and inoculated with *R. intraradices* showed frequently blue coloration in the rhizodermis at early time points (1 and 3 dpi), whereas no GUS activity was observed for the *dmi3-1* and *dmi1-3* mutants (Fig. 4a). Treatments with chitotetraose, chitoheptaose, or NodSm-IV(C16:2, S) for 4 h resulted in a similar blue coloration in rhizodermal cells of WT plants while those of the mutants remained colorless (Fig. 4b). Furthermore, qRT-PCR analysis showed that *MtHEXO2* transcript levels in roots treated with NodSm-IV(C16:2, S) were significantly higher for WT plants than for the mutants (Fig. 4c). *MtHEXO2* transcript levels in roots inoculated with *R. intraradices*, however, did not differ significantly between WT and mutant plants when roots were harvested at 1 dpi or 3 dpi (Fig. S8). Taken together, our analysis of the *dmi3-1* and *dmi1-3* mutants indicates that symbiosis-related *MtHEXO2* induction in the rhizodermis depends on a functional CSSP.

Subcellular localization of MtHEXO2

The SignalP-6.0 computer program predicts a signal peptide of 18 amino acids for MtHEXO2, suggesting that the protein is secreted (Fig. S3). To explore subcellular localization of MtHEXO2 during the early stage of symbiosis with *R. intraradices*, roots of R108 plants were transformed with a binary vector containing the 2628-bp *MtHEXO2* promoter sequence and the *MtHEXO2* coding sequence fused to a C-terminal *RFP* tag (*MtHEXO2*$_{pro}$*-MtHEXO2:RFP*). Roots inoculated with AM fungi were then analyzed by laser scanning confocal microscopy. Red fluorescent signals representing MtHEXO2:RFP could be assigned mainly to rhizodermal cells (atrichoblasts) that were in contact with the fungus while neighboring cortex cells showed no or only weak red fluorescence. Strong fluorescent signals were observed in the cell periphery of the rhizodermal cells, suggesting that MtHEXO2 is an extracellular protein (Fig. 5a,b). No red

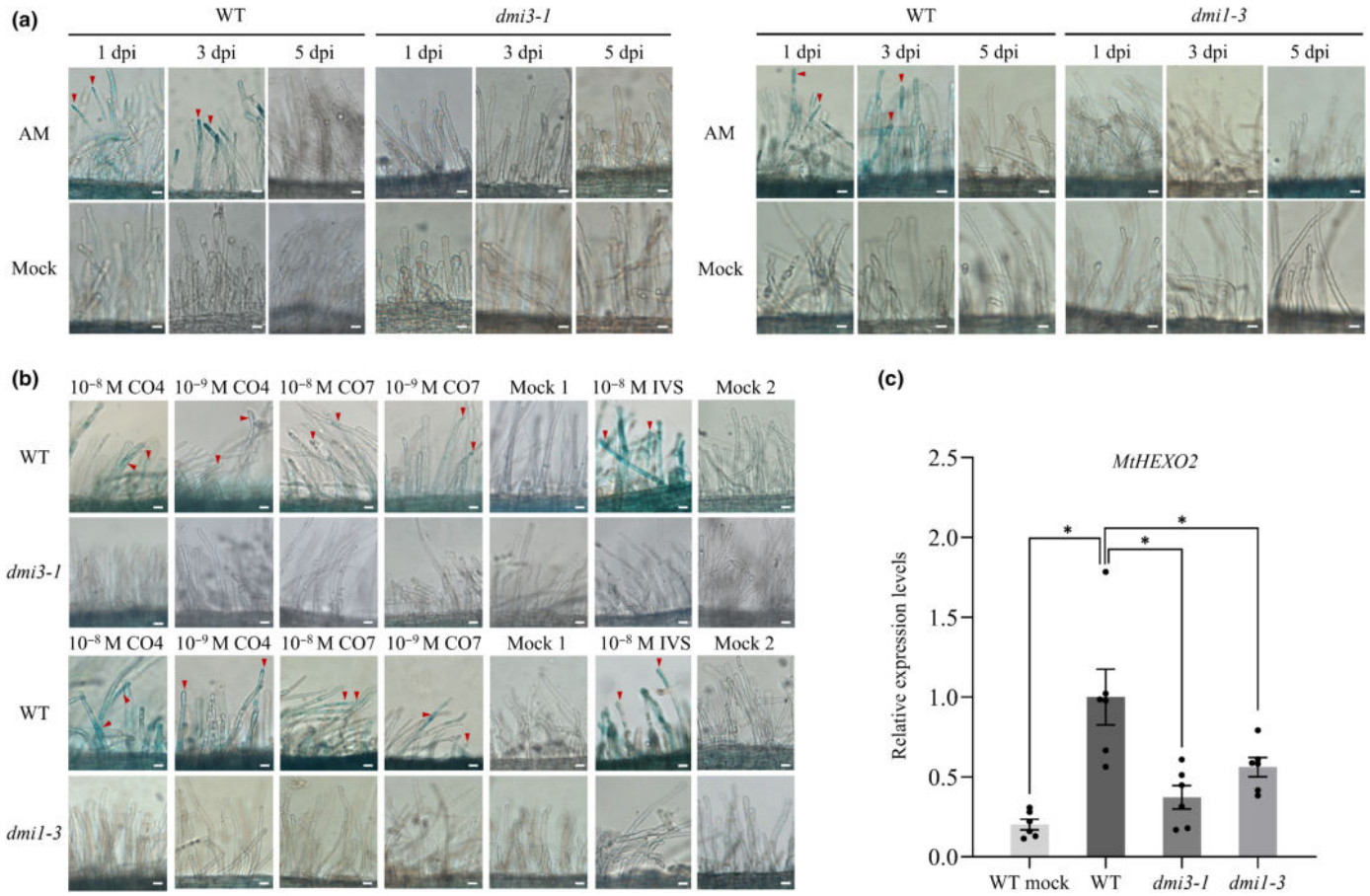

Fig. 4 *MtHEXO2* expression in rhizodermal cells depends on *DMI3* and *DMI1*. (a, b) Analysis for GUS activity in rhizodermal cells of *dmi3-1*, *dmi1-3*, and wild-type (WT) plants (*Medicago truncatula* Jemalong A17) transformed with *MtHEXO2*$_{pro}$*-GUS*. (a) Plants inoculated with *Rhizophagus intraradices* (arbuscular mycorrhizal (AM)) or mock-inoculated with sterilized substrate (Mock) were analyzed at indicated time points after inoculation. Arrowheads mark blue root hairs. (b) Analysis of plants treated with indicated concentrations of chitotetraose (CO4) or chitoheptaose (CO7) dissolved in Jensen medium or with 10^{-8} M NodSm-IV(C16:2, S) dissolved in Jensen medium containing 0.5% (v/v) DMSO (abbreviated as 10^{-8} IVS) for 4 h. Control plants were treated with Jensen medium (Mock 1) or Jensen medium containing 0.5% (v/v) DMSO (Mock 2). Arrowheads mark blue coloration of young root hairs close to the root tip. (c) qRT-PCR analysis of *MtHEXO2* transcripts in roots of WT, *dmi3-1*, and *dmi1-3* plants. Roots of seedlings were immersed for 4 h in Jensen medium containing 0.6 μM NodSm-IV(C16:2, S) and 0.5% (v/v) DMSO. Wild-type plants were also treated with Jensen medium containing 0.5% (v/v) DMSO (WT mock). Root RNA from 8 to 10 plants was analyzed in three pools per genotype. Data indicate means ± SE of normalized expression values ($n = 3$). Asterisks indicate significantly lower *MtHEXO2* expression relative to the induced WT (two-tailed Student's *t*-test: *, *P*-value ≤ 0.05). Bars, 20 μm.

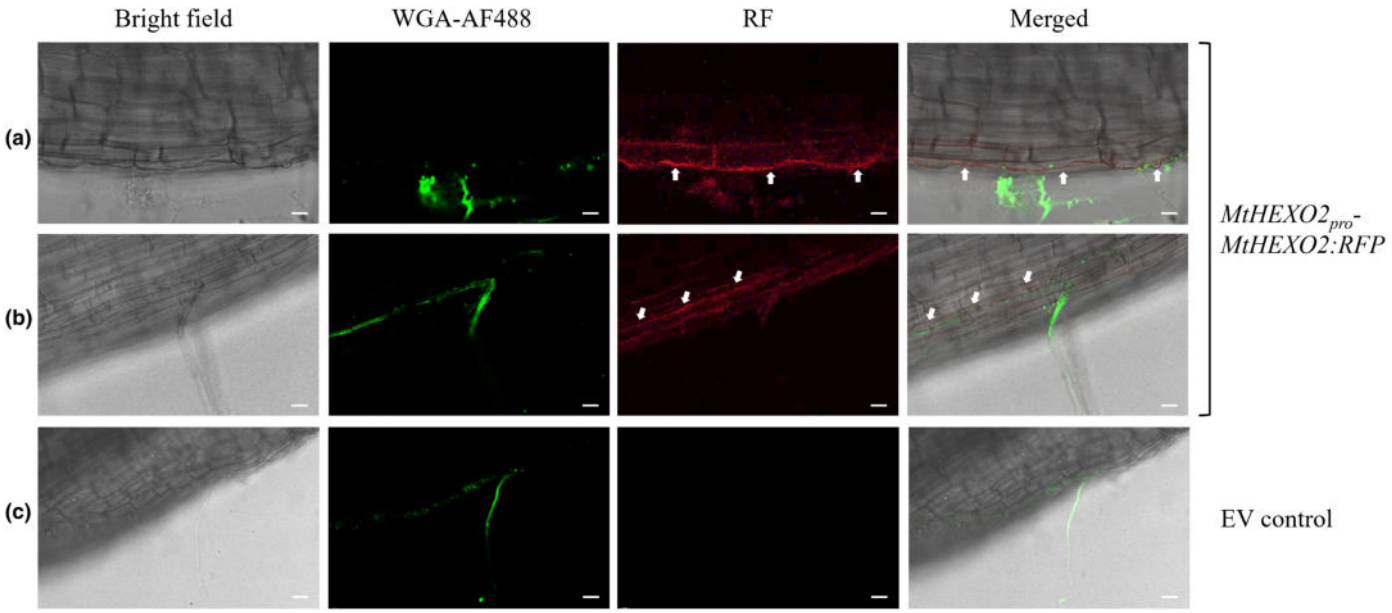

Fig. 5 Subcellular localization of MtHEXO2:RFP in mycorrhizal roots. Roots of *Medicago truncatula* R108 were transformed with a binary vector containing *MtHEXO2*$_{pro}$-*MtHEXO2:RFP* or the empty vector (EV). Transformed roots were inoculated with *Rhizophagus intraradices*, harvested at 8–10 dpi, and analyzed with a confocal laser scanning microscope. *Rhizophagus intraradices* was visualized by using WGA-AF488 (green fluorescent signals). Analysis of red fluorescent signals (RF) indicated the presence of the MtHEXO2:RFP protein in the periphery of rhizodermal cells that were in direct contact with the fungus (arrows). (a, b) Examples of rhizodermal cells transformed with the *MtHEXO2*$_{pro}$-*MtHEXO2:RFP* construct. (c) Empty vector control showing no red fluorescent signals. Bars, 20 μm.

fluorescent signals were observed for rhizodermal cells of inoculated control roots that were transformed with the empty vector lacking *MtHEXO2:RFP* and analyzed under identical microscopic settings (Fig. 5c).

For subcellular localization of MtHEXO2 in root hairs infected with rhizobia, a similar binary vector containing *MtHEXO2* with a C-terminal *GFP* tag was constructed (*MtHEXO2*$_{pro}$-*MtHEXO2:GFP*). Roots of R108 plants transformed with this construct were inoculated with a *S. meliloti* Rm41 derivative constitutively expressing mCherry. Analysis by fluorescence microscopy revealed that MtHEXO2:GFP could be detected for curled root hairs at 2–3 dpi but not for noninfected root hairs. Red fluorescent signal emitted by the rhizobial microcolony in the root hair curl (infection pocket) was typically coinciding with green fluorescent signal from MtHEXO2:GFP, resulting in a yellow area in overlaid images (Fig. 6a–c). Infection threads of root hairs, visualized by the mCherry-expressing bacteria, did not show green fluorescent signals (Fig. 6c). Infected root hairs on control roots transformed with the empty vector (lacking the *MtHEXO2:GFP* construct) showed faint green background fluorescence (Fig. 6d), as root hair curling in *M. truncatula* can lead to the accumulation of autofluorescent material in the curled root hair (Fournier *et al.*, 2015). In conclusion, these results indicate that MtHEXO2 is an extracellular protein that can accumulate in the infection pocket of curled root hairs.

Biochemical analysis of MtHEXO2

The *MtHEXO2* coding sequences of the *M. truncatula* ecotypes Jemalong A17 and R108 share 99% identity of nucleotides and amino acids, respectively (Figs S9, S10). The full-length coding sequences of *MtHEXO2* were cloned from both ecotypes. For expression of a His-tagged protein in *E. coli* BL21(DE3), the coding sequence of *MtHEXO2* from R108 (without the predicted signal peptide) was inserted into pET-28a. As a control version of MtHEXO2 without enzyme activity, a modified construct with two amino acid substitutions (D325A and E326A) was also cloned into pET-28a. Proteins extracted from *E. coli* cells carrying the constructed plasmids were subjected to nickel affinity chromatography, and eluted proteins were analyzed by SDS-PAGE. The His-tagged MtHEXO2 protein was only faintly detected on Western blots when an anti-His antibody was used (Fig. S11). However, expression of a truncated form of MtHEXO2 (residues 119 to 463 with an N-terminal 6xHis tag) resulted in higher production levels of the protein (*c.* 42 kDa band), which was used to immunize a rabbit (Fig. S12). Western blot analysis indicated that the obtained anti-MtHEXO2 antiserum could recognize the recombinant MtHEXO2 protein as well as the D325A/E326A variant (Fig. S13a). The His-tagged MtHEXO2 protein showed hydrolytic activity when *p*-nitrophenyl-*N*-acetyl-β-D-glucosaminide (*p*NP-GlcNAc) was used as substrate. By contrast, no activity was found for the D325A/E326A variant, indicating that these residues are essential for enzyme activity (Fig. S13b).

As MtHEXO2 was only poorly expressed in *E. coli*, we continued research by using *P. pastoris* as an expression system. The *MtHEXO2* sequence of Jemalong A17 (without predicted signal peptide) was cloned into pPIC9K, which contains a yeast signal peptide to allow secretion of the expressed protein. *P. pastoris* GS115 transformed with the empty vector pPIC9K was used as a

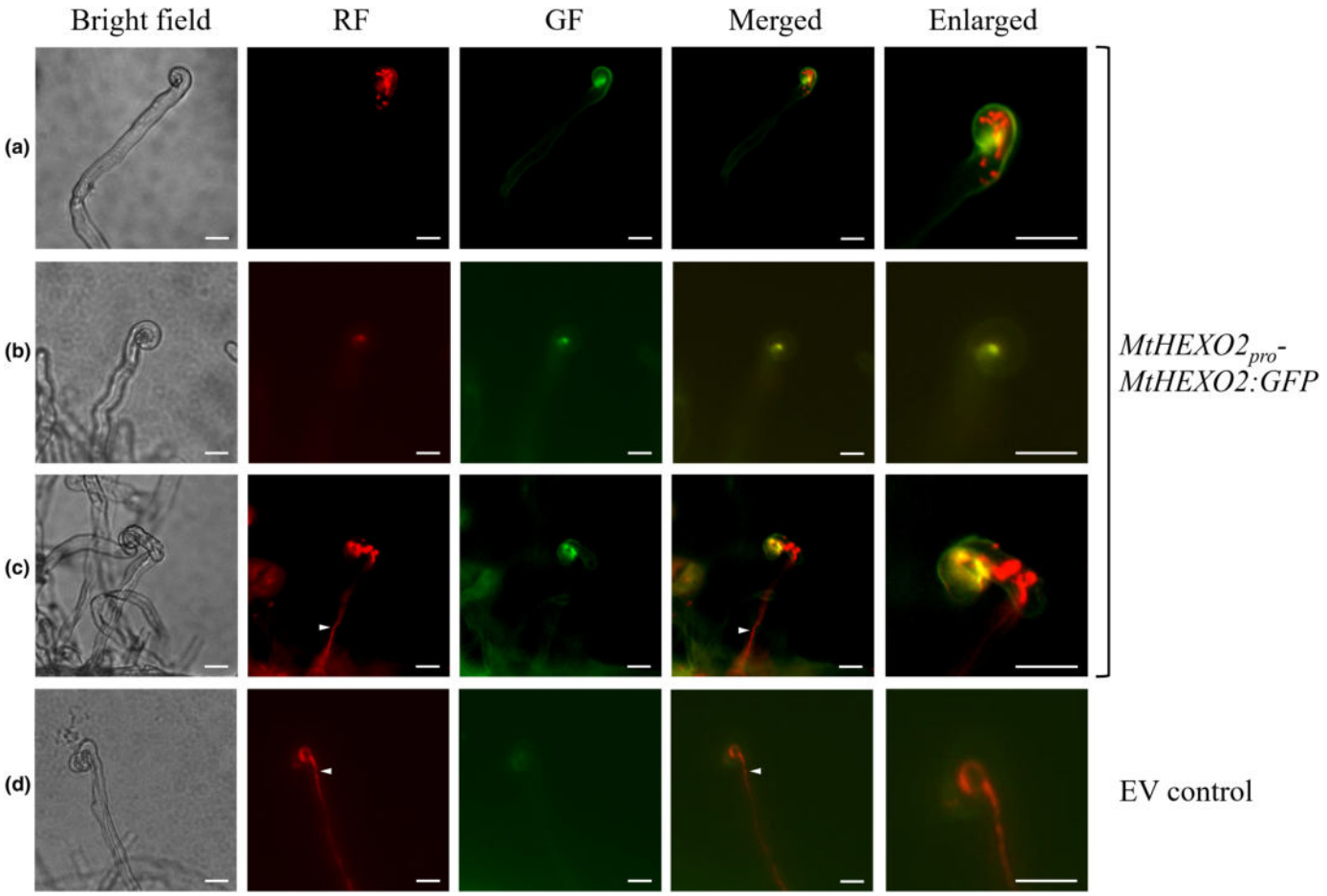

Fig. 6 Subcellular localization of MtHEXO2:GFP in root hairs inoculated with rhizobia. Roots of *Medicago truncatula* R108 were transformed with a binary vector containing *MtHEXO2*$_{pro}$-*MtHEXO2:GFP* or the empty vector (EV). Transformed roots were inoculated with *Sinorhizobium meliloti* Rm41 constitutively expressing mCherry. Root hairs of roots harvested at 3 dpi were analyzed with a fluorescence microscope. The yellow color in merged images (see enlarged images for details) indicates an overlap of MtHEXO2:GFP signals (GF, green fluorescence) with fluorescent signals of rhizobia (RF, red fluorescence). (a, b) Examples of MtHEXO2:GFP accumulation in infection pockets of a curled root hairs before infection thread development. (c) Accumulation of MtHEXO2:GFP in the infection pocket of a curled root hair that has developed an infection thread. (d) Control images showing a curled root hair of a root transformed with the empty vector without the *MtHEXO2:GFP* construct. Arrowheads (in c, d) mark formed infection threads. Bars, 20 µm.

negative control. Culture supernatants containing recombinant MtHEXO2 protein were collected by centrifugation and then directly used for SDS-PAGE and Western blot analysis with the prepared anti-MtHEXO2 antiserum. A band of the predicted molecular weight (*c.* 68 kDa) was clearly visible, indicating that MtHEXO2 was successfully expressed and secreted by *P. pastoris* (Fig. 7a). The protein was then used for enzyme tests with various aryl glycoside substrates. Culture supernatants containing MtHEXO2 efficiently hydrolyzed the *p*NP-GlcNAc and *p*-nitrophenyl-*N*-acetyl-β-D-galactosaminide (*p*NP-GalNAc) substrates. By contrast, no or only very weak activity comparable to the empty vector control was found with *p*NP-α-L-arabinofuranoside, *p*NP-α-L-arabinopyranoside, *p*NP-β-D-xylopyranoside, *p*NP-β-D-glucopyranoside, or *p*NP-β-D-galactopyranoside (Fig. 7b). These data indicate that MtHEXO2 possesses β-*N*-acetylglucosaminidase and β-*N*-acetylgalactosaminidase activities.

To further characterize the enzyme activity, chitotetraose, chitopentaose, chitohexaose, and chitoheptaose were used as substrates for MtHEXO2 secreted by *P. pastoris*. GlcNAc released from these COs was detected using the DMAB reagent. The results showed that these COs could be degraded by MtHEXO2, whereas no activity was found for control samples from culture supernatants of *P. pastoris* cells carrying the empty vector (Figs 7c, S14). To substantiate these findings, chitopentaose was incubated with MtHEXO2 for different periods and reaction mixtures were separated by reverse-phase HPLC on an amino column. The results indicated that MtHEXO2 was able to completely degrade chitopentaose into GlcNAc. When a shorter incubation time was used, intermediate products, namely chitotetraose, chitotriose, and chitobiose, were observed, while no activity was detected for control samples from culture supernatants of *P. pastoris* cells carrying the empty vector (Fig. 7d). Hence, MtHEXO2 stepwise releases GlcNAc from COs.

As reported previously (Tian *et al.*, 2013; Cai *et al.*, 2018), MtNFH1 of *M. truncatula* can cleave LCOs from *S. meliloti* into lipo-disaccharides and sulfated COs. By contrast to MtNFH1, recombinant MtHEXO2 secreted by *P. pastoris* cleaved neither NodSm-IV(C16:2, S) from *S. meliloti* (Fig. S15), nor LCOs

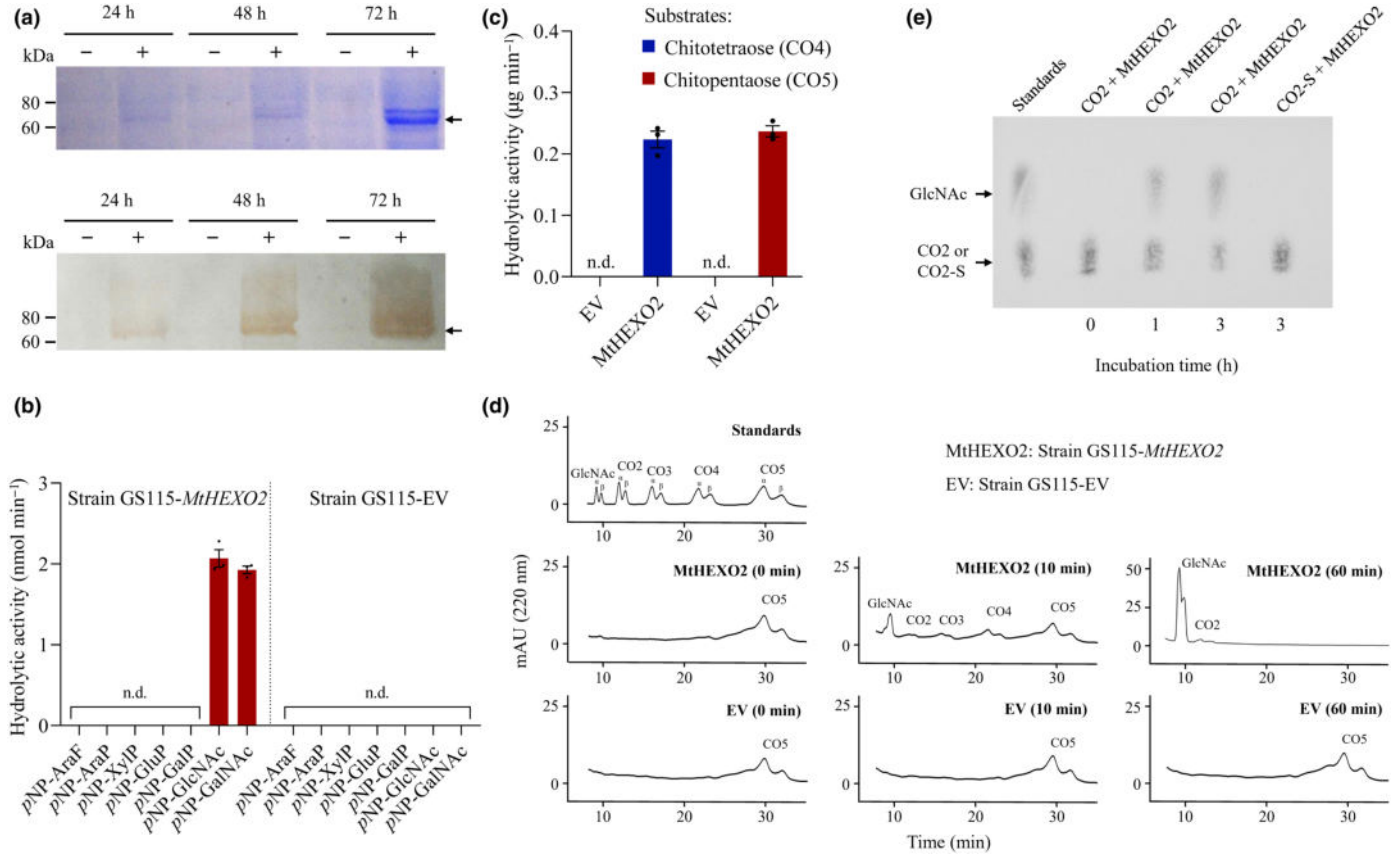

Fig. 7 Biochemical analysis of MtHEXO2 expressed in *Pichia pastoris*. (a) SDS-PAGE (top) and Western blot analysis (bottom) of secreted MtHEXO2 produced by *P. pastoris* expressing *MtHEXO2* (GS115-*MtHEXO2*; lanes marked with +), and the empty vector control (GS115-EV; lanes marked with –). Proteins (16 μl culture supernatant) were analyzed at different times after induction of cells with methanol. Western blot analysis was performed with an antiserum against MtHEXO2. The MtHEXO2 protein (*c.* 68 kDa) is marked by an arrow. (b) Hydrolytic activity of proteins (10 μl culture supernatant) from GS115-*MtHEXO2* and GS115-EV toward aryl glycosides. Data indicate means ± SE from three independent replicates (nd, activity not detected). Abbreviations of aryl glycosides: *p*NP-AraF, *p*-nitrophenyl-α-L-arabinofuranoside; *p*NP-AraP, *p*-nitrophenyl-α-L-arabinopyranoside; *p*NP-XylP, *p*-nitrophenyl-β-D-xyloside; *p*NP-GluP, *p*-nitrophenyl-β-D-glucopyranoside; *p*NP-GalP, *p*-nitrophenyl-β-D-galactopyranoside; *p*NP-GlcNAc, *p*-nitrophenyl-*N*-acetyl-β-D-glucosaminide; *p*NP-GalNAc, *p*-nitrophenyl-*N*-acetyl-β-D-galactosaminide. (c) Results of similar tests with chitooligosaccharides (COs) (1 mM chitotetraose or chitopentaose) as substrates. Produced GlcNAc was photometrically determined with the DMAB reagent. Data indicate means ± SE from three independent replicates. (d) High-pressure liquid chromatography Chitopentaose (10 mM) was incubated with 10 μl culture supernatant from GS115-*MtHEXO2* for indicated periods. Supernatants from the GS115-EV strain (EV) lacked CO-cleaving activity. Commercially available COs were used as standards (GlcNAc; CO2, chitobiose; CO3, chitotriose; CO4; chitotetraose; CO5, chitopentaose). (e) Sulfated chitobiose was not cleaved by MtHEXO2. Chitobiose (abbreviated as CO2) or sulfated chitobiose (abbreviated as CO2-S) were incubated with 10 μl culture supernatant from GS115-*MtHEXO2* for different periods, and the products were analyzed on TLC plates. GlcNAc and chitobiose were used as standards (left lane).

from *Sinorhizobium* sp. NGR234 (Fig. S16), indicating that the acyl chain at the nonreducing end protects the LCO carbohydrate backbone from degradation by MtHEXO2.

We also asked whether structural modifications at the reducing end of COs can influence CO hydrolysis by MtHEXO2. Recombinant MtNFH1 (expressed in *E. coli*) was used to hydrolyze NodSm-IV(C16:2, S), and the resulting sulfated chitobiose was separated from the lipo-disaccharide NodSm-II(C16:2) by butanol extraction. Recombinant MtHEXO2 secreted by *P. pastoris* was then incubated with chitobiose or the prepared sulfated chitobiose. TLC analysis of the reaction mixtures showed that chitobiose was partially converted into GlcNAc, whereas sulfated chitobiose was not hydrolyzed under the test conditions used (Fig. 7e). These findings suggest that the sulfate group at the reducing end of chitobiose protects the molecule from cleavage by MtHEXO2.

Mutants with a *Tnt1* insertion in *MtHEXO2* show decreased colonization by AM fungi

To investigate the biological function of *MtHEXO2* during symbiosis, two *Tnt1* retrotransposon insertion mutant lines (NF4082 and NF5709) of *M. truncatula* R108 were obtained from the mutant collection at Oklahoma State University. PCR analyses and sequencing results confirmed that both lines contained a *Tnt1* retrotransposon insertion in the first exon of *MtHEXO2* (660 bp and 523 bp downstream of the ATG start, respectively). Homozygous lines were selected and named *hexo2-1* and *hexo2-2* (Figs 8a, S17a,b). Under our growth conditions, the mutant plants grew normally and could not be phenotypically distinguished from WT plants. Further characterization by qRT-PCR and reverse transcription PCR showed that *MtHEXO2* transcript

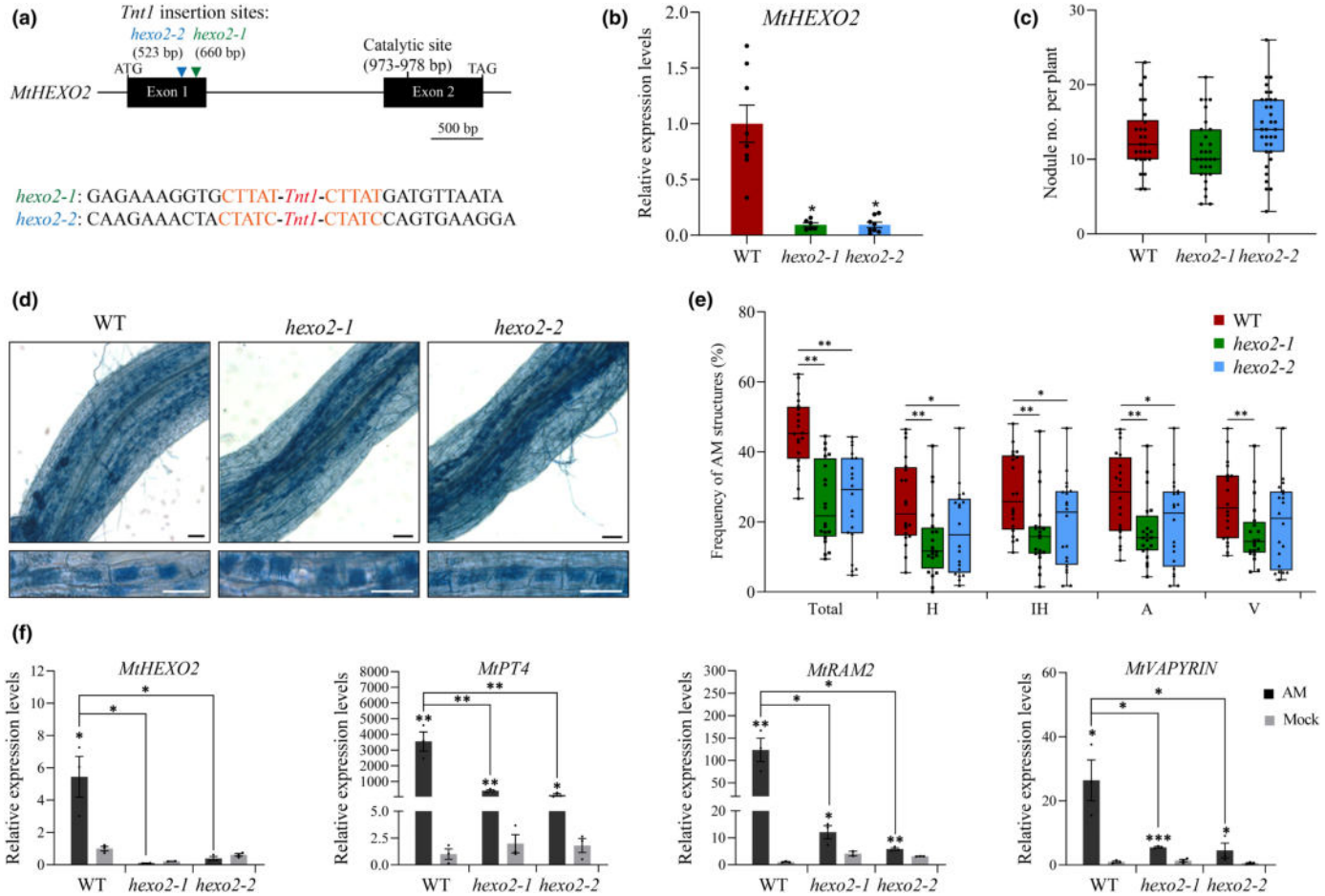

Fig. 8 *Hexo2* mutants show reduced colonization by arbuscular mycorrhizal (AM) fungi. (a) Schematic view of *Tnt1* insertion sites of the *hexo2-1* and *hexo2-2* mutants of *Medicago truncatula* R108. The duplication sequence flanking the *Tnt1* sequence is marked in orange. (b) Analysis of *MtHEXO2* expression by qRT-PCR in wild-type (WT) and the *hexo2* mutants. Roots from 4-wk-old plants were used for each RNA extraction (at least 3 RNA extractions per genotype; $n \geq 3$). Data indicate means ± SE of normalized expression values. (c) Nodule number of WT and *hexo2* mutant plants inoculated with *S. meliloti* Rm41 (21 dpi). Data are shown as boxplots (≥25 plants from two independent experiments; $n \geq 25$). (d–f) Analysis of plants inoculated with *Rhizophagus intraradices* (30 dpi). (d) Pictures illustrating mycorrhizal roots (upper; bars, 100 μm) and arbuscular cells (lower; bars, 50 μm) in WT and *hexo2* plants. (e) Quantification of AM structures in mycorrhizal roots as in (d). H, hyphopodia; IH, internal hyphae; A, arbuscules; V, vesicles. Data are shown as boxplots (20 plants from three independent experiments; $n = 20$). (f) Quantitative real-time-PCR analysis of *MtHEXO2* and symbiosis-related marker genes in mycorrhizal roots of WT and *hexo2* mutants. Each RNA sample was obtained from 3 to 4 pooled plants. Data indicate means ± SE of normalized expression values ($n = 3$). Asterisks above columns indicate a significantly increased gene expression in mycorrhizal roots (AM) compared with control roots (Mock). Statistical differences between genotypes in (b, e, f) are indicated by asterisks above lines (two-tailed Student's *t*-test: *, *P*-value ≤ 0.05; **, *P*-value ≤ 0.01). Boxplots in (c, e) show datapoints, median (horizontal line), lower/upper quantile (box), and lower/upper 1.5 times interquartile range (whiskers).

levels in these mutants were significantly decreased compared with the WT (Figs 8b, S17c).

To uncover a possible symbiotic function of *MtHEXO2*, nodulation tests with *S. meliloti* Rm41 were performed. The results did not reveal obvious differences between mutant and WT plants under the test conditions used (Fig. 8c; Table S3). However, differences between WT and *hexo2* plants were seen when the plants were inoculated with *R. intraradices*. Although fungal root colonization was observed in both WT and *hexo2* plants, results from three independent experiments showed that the frequency of AM structures was significantly lower in *hexo2* roots (Fig. 8d,e; Table S4). Gene expression analysis by qRT-PCR showed that expression of *MtHEXO2* and AM symbiosis-related marker genes was reduced in mycorrhizal roots of *hexo2* mutants (Fig. 8f), while expression of defense-related genes (*PR4* and chitinase genes) did not significantly differ from WT plants (Fig. S18).

To test for gain-of-function phenotypes, we used *A. tumefaciens*-mediated transformation to generate stably transformed *M. truncatula* R108 plants constitutively overexpressing *MtHEXO2* under the control of a double CaMV 35S promoter. Expression of *MtHEXO2* analyzed by qRT-PCR was increased about fivefold in transformants compared with WT plants. We then inoculated the roots with AM fungi and compared the *MtHEXO2*-overexpressing transformants with WT and *hexo2-1* mutant plants. The results showed that fungal colonization was not significantly different (Fig. S19; Table S5).

To confirm that reduced fungal colonization in the *hexo2* mutants was due to *MtHEXO2*, a full-length *MtHEXO2* (R108)

construct (including the 2628-bp promoter sequence) and an *RFP* expression cassette were expressed in roots of *hexo2* mutants. Transformation with the empty vector (containing only the *RFP* expression cassette) was used as a control. Transformation efficiency data are shown in Table S6. Roots showing red fluorescence were subjected to qRT-PCR and reverse transcription PCR analysis. The results confirmed the expression of *MtHEXO2* in the roots of transformed *hexo2* mutants (Figs 9a, S20). Furthermore, plants with roots showing red fluorescence were inoculated with *R. intraradices* and roots harvested 30 d later. The degree of fungal colonization was increased in both *hexo2* mutants, that is, the WT phenotype was restored. By contrast, mutants transformed with the empty vector control retained weak fungal colonization (Fig. 9b; Table S7). To test whether GlcNAc, the end product of MtHEXO2 activity, is required for efficient symbiosis, we attempted to restore WT colonization levels in *hexo2* mutants by adding exogenous GlcNAc. However, even a repeated treatment of *hexo2* mutant roots with 1 mM GlcNAc had no obvious effect on fungal root colonization (Fig. S21).

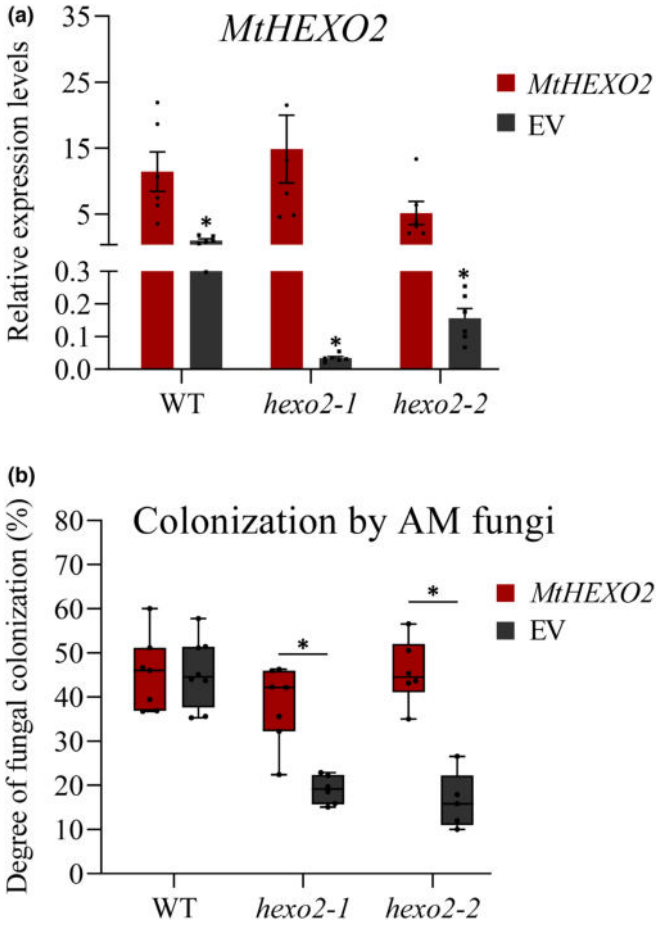

Fig. 9 Functional complementation of *hexo2* mutants by *MtHEXO2* expression under the control of the native promoter. (a) Quantitative real-time-PCR analysis of transformed *hexo2* mutant roots showing *MtHEXO2* expression as in wild-type (WT) plants (red columns) in contrast to empty vector (EV) controls (black columns). In addition, WT plants were transformed with the *MtHEXO2* construct or the empty vector. Each RNA sample was obtained from 3 to 4 pooled plants. Data indicate means ± SE ($n = 3$). (b) Root colonization by *Rhizophagus intraradices* in *hexo2* roots expressing *MtHEXO2* (30 dpi) using 5–8 transformants ($5 \leq n \leq 8$). Complemented mutants showed similar fungal colonization as the WT transformed with the empty vector. Transformation of WT plants with the *MtHEXO2* construct showed no effect on fungal colonization. Boxplots show datapoints, median (horizontal line), lower/upper quantile (box), and lower/upper 1.5 times interquartile range (whiskers). Asterisks in panels a and b indicate significant differences between transformants and empty vector controls (two-tailed Student's *t*-test: *, *P*-value ≤ 0.01).

Discussion

In this study, we identified and characterized MtHEXO2, a GH20 enzyme of *M. truncatula* that efficiently hydrolyzes COs. Mutant analysis indicated that MtHEXO2 has a function in AM symbiosis but not in nodule symbiosis. Expression of *MtHEXO2* in *M. truncatula* roots was found to be induced during symbiosis with AM fungi and rhizobia. Promoter-*GUS* analysis revealed that rhizodermal cells, particularly root hairs, show an induction of *MtHEXO2* expression in response to fungal inoculation. Analysis of mycorrhizal roots at later symbiotic stages indicated that *MtHEXO2* expression in the root cortex coincides with fungal structures, particularly arbuscules, suggesting that MtHEXO2 may act locally at the symbiotic interface to hydrolyze fungal COs derived from chitin in the fungal cell wall (Bonfante-Fasolo *et al.*, 1990). Future studies should clarify whether homeostasis of CO levels affects the formation and/or maintenance of arbuscules in *M. truncatula* and other plants. The finding that LCO receptor genes are expressed in arbuscule-containing cells in various plants (Gomez *et al.*, 2009; Rasmussen *et al.*, 2016; Girardin *et al.*, 2019) suggests that expression of *HEXO2* genes in these cells depends on a functional CSSP. When *M. truncatula* was inoculated with *S. meliloti*, induction of the *MtHEXO2* promoter activity was transiently induced in root hairs at 1 dpi (Fig. 2). Elevated *MtHEXO2* expression in response to *S. meliloti* inoculation was also observed in previous studies, albeit at later time points (Benedito *et al.*, 2008; Breakspear *et al.*, 2014; Liu *et al.*, 2019; Schiessl *et al.*, 2019). Treatments of roots with COs, NodSm-IV(C16:2, S), or LCOs from *Sinorhizobium* sp. NGR234 resulted in a similar induction of *MtHEXO2* promoter activity. Induced *MtHEXO2* expression in rhizodermal cells of plants treated with *S. meliloti* LCOs has been previously reported by Jardinaud *et al.* (2016) (Fig. S2). Induction of the *MtHEXO2* promoter activity in root hairs by COs and NodSm-IV(C16:2, S) was found to be CSSP-dependent in our study, since *dmi3-1* and *dmi1-3* mutants showed no response.

Localization experiments with roots inoculated with AM fungi revealed the detection of fluorescent MtHEXO2:RFP protein in rhizodermal cells that were in contact with fungal hyphae, while no red fluorescent signals were observed in cortex cells at 8–10 dpi (Fig. 5). These results suggest that MtHEXO2 is released into the apoplast or associated with the outer leaflet of the plasma membrane in rhizodermal cells. Accordingly, MtHEXO2 in arbuscule-containing cells is expected to accumulate in the symbiotic interface compartment between the fungus and the peri-fungal membrane of the host plant. Analysis of subcellular localization was further performed on *S. meliloti*-infected root hairs expressing green fluorescent MtHEXO2:GFP. The yellow

signals in overlay images of Fig. 6(a–c) indicate co-localization of MtHEXO2:GFP and mCherry-expressing *S. meliloti* bacteria in the infection pocket of three independent curled root hairs. Focal exocytosis of proteins into the infection pocket of curled root hairs was previously reported for various symbiosis-related proteins, including MtNFH1/MtCHIT5b (Fournier *et al.*, 2015; Cai *et al.*, 2018; Li *et al.*, 2022). In conclusion, our subcellular localization analysis indicates that MtHEXO2 is an extracellular enzyme which comes into direct contact with molecules secreted by AM fungi and rhizobia.

Analysis of recombinant protein expressed in *E. coli* and *P. pastoris* indicated that MtHEXO2 is a functional β-hexosaminidase that cleaves *p*NP-GlcNAc, *p*NP-GalNAc, and COs in a similar way as β-hexosaminidase purified from jack bean (*Canavalia ensiformis*) and GH20 enzymes of *A. thaliana* (Li & Li, 1970; Gutternigg *et al.*, 2007; Strasser *et al.*, 2007; Fig. 7). LCOs were not cleaved by MtHEXO2, which is consistent with observations that GH20 enzymes are *exo*-glycosidases that release terminal GlcNAc or GalNAc from the nonreducing end of oligosaccharides (Liu *et al.*, 2018; Drula *et al.*, 2022). In contrast to chitobiose, sulfated chitobiose, that is, the hydrophilic cleavage product of the LCO-cleaving hydrolases MtNFH1/MtCHIT5b (Tian *et al.*, 2013; Cai *et al.*, 2018; Li *et al.*, 2022), was not hydrolyzed by MtHEXO2 under our test conditions, suggesting that sulfated chitobiose accumulates in the rhizosphere of *M. truncatula* or is hydrolyzed by an unknown enzyme. In this context, it is worth mentioning that certain rhizobia and fungi produce LCOs without reducing end modifications (Spaink *et al.*, 1991; Maillet *et al.*, 2011; Rush *et al.*, 2020). When such LCOs are degraded by plant hydrolases (Heidstra *et al.*, 1994), the hydrophilic cleavage products are chitobiose or chitotriose and thus likely substrates for GH20 enzymes.

As *MtHEXO2* expression was regulated by LCO signaling and MtHEXO2:GFP was detected in infection pockets of root hairs, we initially hypothesized that MtHEXO2 could play a role in the nodule symbiosis. However, nodulation of *hexo2* roots was similar to that of WT plants. These results are consistent with our findings that rhizobial LCOs are not cleaved by MtHEXO2. Although MtHEXO2 appears to be not essential for the nodule formation, minor quantitative symbiotic effects of MtHEXO2 cannot be completely ruled out as HEXO2 may recognize unknown GlcNAc or GalNAc containing plant substrates. For example, GH20 enzymes were found to release terminal GlcNAc or GalNAc residues of *N*-glycans (Gutternigg *et al.*, 2007; Strasser *et al.*, 2007; Alvisi *et al.*, 2021) and thus may have the potential to modify properties of symbiotic LysM receptors, which are known to be *N*-glycosylated (Broghammer *et al.*, 2012; Lefebvre *et al.*, 2012). In our study, strong constitutive GUS activity reflecting *MtHEXO2* promoter activity was observed in the central cylinder of roots (Fig. 1) and in vascular tissue of nodules (Fig. 2). We speculate that *MtHEXO2* expression in vascular tissues is associated with processing of *N*-glycans that may accumulate in the xylem sap (Boulanger *et al.*, 2014; Tsujimori *et al.*, 2019).

Hexo2 mutants showed reduced colonization by AM fungi (Fig. 8), which could be complemented by a WT *HEXO2* copy (Fig. 9). We suggest that the symbiosis-promoting effect of MtHEXO2 is due to inactivation of fungal COs once CSSP-mediated *MtHEXO2* expression is induced by COs or LCOs. Too strong and continuous stimulation of the CSSP could eventually result in autoregulation responses that negatively affect the AM symbiosis (Staehelin *et al.*, 2011). In this view, the signal-inactivating function of MtHEXO2 during the AM symbiosis would be a feedback response, which is similar to the rhizobial LCO inactivation by MtNFH1/MtCHIT5b in the nodule symbiosis (Cai *et al.*, 2018; Li *et al.*, 2022). MtHEXO2 can hydrolyze long-chain COs such as chitohexaose and chitoheptaose, thereby transiently producing short-chain COs (Figs 3, S14). These findings suggest that MtHEXO2 can not only regulate CO levels but also affect the ratio of long-chain COs to short-chain COs during the AM symbiosis. Enzymatic inactivation of excess amounts of COs, especially long-chain COs, could play a role in suppressing plant defense reactions as COs are known to trigger defense responses via the classic chitin signaling pathway (Bozsoki *et al.*, 2017; Khokhani *et al.*, 2021). However, mycorrhizal roots of *hexo2* mutants and WT plants did not show significant differences in the expression of plant defense genes in our qRT-PCR analysis (Fig. S18) and further experiments are required to explore plant defense reactions during AM symbiosis. It is worth noting in this context that RiSLM, a LysM effector of the AM fungus *R. irregularis*, can sequester COs and promote the symbiosis with *M. truncatula* (Zeng *et al.*, 2020). Thus, fungal effectors and host enzymes such as MtHEXO2 may both reduce CO levels at the symbiotic interface by different mechanisms.

Overexpression of the LCO-cleaving hydrolase gene *MtCHIT5b* resulted in reduced nodulation of *M. truncatula* roots (Li *et al.*, 2022). However, overexpression of *MtHEXO2* did not affect root colonization by AM fungi in this study. It can be assumed that CO levels at the symbiotic interface decrease with increasing amounts of MtHEXO2, while LCO levels are expected to remain unchanged. In *MtHEXO2*-overexpressing plants, fungal LCOs might therefore be sufficient to trigger CSSP-mediated gene expression and subsequent symbiosis with AM fungi.

What is the fate of GlcNAc produced by MtHEXO2? CO-derived GlcNAc could be recycled by AM fungi and act as a signal molecule to localize the presence of a susceptible host (Kobae *et al.*, 2015; Nadal *et al.*, 2017). On the contrary, GlcNAc at the symbiotic interface could be also taken up by the host plant via GlcNAc-specific transporter proteins. Remarkably, roots of rice and maize mutants defective in a GlcNAc transporter (*nope1* mutants) showed significantly reduced colonization by AM fungi (Paszkowski *et al.*, 2006; Nadal *et al.*, 2017).

In conclusion, our study highlights that *MtHEXO2* is a symbiosis-related gene that promotes AM symbiosis. Rhizodermal *MtHEXO2* expression depends on a functional CSSP that could be activated by COs and LCOs. MtHEXO2 is an extracellular β-hexosaminidase that can efficiently hydrolyze COs and thus likely plays a crucial role in inactivation of fungal COs in the symbiotic interface.

Acknowledgements

We are grateful to Qi Sun, Christian Wagner, and Yan Wang (Sun Yat-sen University) for their help with various aspects of this work. We thank Clare Gough (INRAE-CNRS, Castanet-Tolosan, France) for the *dmi3-1* and *dmi1-3* mutants and William J. Broughton (University of Geneva, Switzerland) for NGR234 and NGRΔ*nodABC*. Eva Kondorosi and Michael Schultze (CNRS, Gif-sur-Yvette, France) kindly provided pISV2678 and *S. meliloti* 1021 (pEK327). This work was supported by the Sino-Swiss Science and Technology Cooperation Programme (grant 32161133026 from the National Natural Science Foundation of China to CS; grant no. IZLCZ0-206026 from the Swiss National Science Foundation to DR). Work in Guangzhou was also supported by the National Natural Science Foundation of China (grant 31670241 to CS), the Science Foundation of the State Key Laboratory of Biocontrol, and the Guangdong Key Laboratory of Plant Resources.

Competing interests

None declared.

Author contributions

Y-HW, WL, JC and R-JL performed research. JW and KSM screened for the *hexo2* mutants and provided seeds. Y-HW, WL, JC, R-JL, Z-PX, DR and CS analyzed data; Y-HW, WL, Z-PX, DR and CS conceived the work; Y-HW, DR and CS wrote the paper.

ORCID

Wei Liu https://orcid.org/0000-0002-5693-4086
Kirankumar S. Mysore https://orcid.org/0000-0002-9805-5741
Didier Reinhardt https://orcid.org/0000-0003-3495-6783
Christian Staehelin https://orcid.org/0000-0002-0719-7251
Jiangqi Wen https://orcid.org/0000-0001-5113-7750
Zhi-Ping Xie https://orcid.org/0000-0002-8855-0036

Data availability

The data supporting the findings of this study are available in the Supporting Information of this article.

References

Afkhami ME, Stinchcombe JR. 2016. Multiple mutualist effects on genome-wide expression in the tripartite association between *Medicago truncatula*, nitrogen-fixing bacteria and mycorrhizal fungi. *Molecular Ecology* **25**: 4946–4962.

Alvisi N, van Noort K, Dwiani S, Geschiere N, Sukarta O, Varossieau K, Nguyen DL, Strasser R, Hokke CH, Schots A *et al.* 2021. β-Hexosaminidases along the secretory pathway of *Nicotiana benthamiana* have distinct specificities toward engineered helminth *N*-glycans on recombinant glycoproteins. *Frontiers in Plant Science* **12**: 638454.

Benedito VA, Torres-Jerez I, Murray JD, Andriankaja A, Allen S, Kakar K, Wandrey M, Verdier J, Zuber H, Ott T *et al.* 2008. A gene expression atlas of the model legume *Medicago truncatula*. *The Plant Journal* **55**: 504–513.

Boisson-Dernier A, Chabaud M, Garcia F, Bécard G, Rosenberg C, Barker DG. 2001. *Agrobacterium rhizogenes*-transformed roots of *Medicago truncatula* for the study of nitrogen-fixing and endomycorrhizal symbiotic associations. *Molecular Plant–Microbe Interactions* **14**: 695–700.

Bonfante-Fasolo P, Faccio A, Perotto S, Schubert A. 1990. Correlation between chitin distribution and cell wall morphology in the mycorrhizal fungus *Glomus versiforme*. *Mycological Research* **94**: 157–165.

Boulanger A, Zischek C, Lautier M, Jamet S, Rival P, Carrere S, Arlat M, Lauber E. 2014. The plant pathogen *Xanthomonas campestris* pv. *campestris* exploits *N*-acetylglucosamine during infection. *mBio* **5**: e01527-14.

Bozsoki Z, Cheng J, Feng F, Gysel K, Vinther M, Andersen KR, Oldroyd G, Blaise M, Radutoiu S, Stougaard J. 2017. Receptor-mediated chitin perception in legume roots is functionally separable from Nod factor perception. *Proceedings of the National Academy of Sciences, USA* **114**: E8118–E8127.

Bozsoki Z, Gysel K, Hansen SB, Lironi D, Krönauer C, Feng F, de Jong N, Vinther M, Kamble M, Thygesen MB *et al.* 2020. Ligand-recognizing motifs in plant LysM receptors are major determinants of specificity. *Science* **369**: 663–670.

Breakspear A, Liu C, Roy S, Stacey N, Rogers C, Trick M, Morieri G, Mysore KS, Wen J, Oldroyd GED *et al.* 2014. The root hair "infectome" of *Medicago truncatula* uncovers changes in cell cycle genes and reveals a requirement for auxin signaling in rhizobial infection. *Plant Cell* **26**: 4680–4701.

Broghammer A, Krusell L, Blaise M, Sauer J, Sullivan JT, Maolanon N, Vinther M, Lorentzen A, Madsen EB, Jensen KJ *et al.* 2012. Legume receptors perceive the rhizobial lipochitin oligosaccharide signal molecules by direct binding. *Proceedings of the National Academy of Sciences, USA* **109**: 13859–13864.

Cai J, Zhang LY, Liu W, Tian Y, Xiong JS, Wang YH, Li RJ, Li HM, Wen JQ, Mysore KS *et al.* 2018. Role of the Nod factor hydrolase MtNFH1 in regulating Nod factor levels during rhizobial infection and in mature nodules of *Medicago truncatula*. *Plant Cell* **30**: 397–414.

Capoen W, Sun J, Wysham D, Otegui MS, Venkateshwaran M, Hirsch S, Miwa H, Downie JA, Morris RJ, Ané J-M *et al.* 2011. Nuclear membranes control symbiotic calcium signaling of legumes. *Proceedings of the National Academy of Sciences, USA* **108**: 14348–14353.

Carrere S, Verdier J, Gamas P. 2021. MtExpress, a comprehensive and curated RNAseq-based gene expression atlas for the model legume *Medicago truncatula*. *Plant and Cell Physiology* **62**: 1494–1500.

Castilho A, Windwarder M, Gattinger P, Mach L, Strasser R, Altmann F, Steinkellner H. 2014. Proteolytic and *N*-glycan processing of human α1-antitrypsin expressed in *Nicotiana benthamiana*. *Plant Physiology* **166**: 1839–1851.

Catoira R, Galera C, de Billy F, Penmetsa RV, Journet EP, Maillet F, Rosenberg C, Cook D, Gough C, Dénarié J. 2000. Four genes of *Medicago truncatula* controlling components of a Nod factor transduction pathway. *Plant Cell* **12**: 1647–1666.

Chabaud M, Boisson-Dernier A, Zhang J, Taylor CG, Yu O, Barker DG. 2006a. *Agrobacterium rhizogenes*-mediated root transformation. In: Mathesius U, Journet EP, Sumner LW, eds. Medicago truncatula *handbook*. Ardmore, OK, USA: Noble Research Institute.

Chabaud M, Harrison M, de Carvalho-Niebel F, B'ecard G, Barker DG. 2006b. Inoculation and growth with mycorrhizal fungi. In: Mathesius U, Journet EP, Sumner LW, eds. Medicago truncatula *handbook*. Ardmore, OK, USA: Noble Research Institute.

Chen S, Songkumarn P, Liu J, Wang GL. 2009. A versatile zero background T-vector system for gene cloning and functional genomics. *Plant Physiology* **150**: 1111–1121.

Crosino A, Genre A. 2022. Peace talks: symbiotic signaling molecules in arbuscular mycorrhizas and their potential application. *Journal of Plant Interactions* **17**: 824–839.

Damiani I, Drain A, Guichard M, Balzergue S, Boscari A, Boyer JC, Brunaud V, Cottaz S, Rancurel C, Da Rocha M *et al.* 2016. Nod factor effects on root hair-specific transcriptome of *Medicago truncatula*: focus on plasma membrane

transport systems and reactive oxygen species networks. *Frontiers in Plant Science* 7: 794.

Drula E, Garron ML, Dogan S, Lombard V, Henrissat B, Terrapon N. 2022. The carbohydrate-active enzyme database: functions and literature. *Nucleic Acids Research* **50**: D571–D577.

Ehrhardt DW, Wais R, Long SR. 1996. Calcium spiking in plant root hairs responding to rhizobium nodulation signals. *Cell* **85**: 673–681.

Elfstrand M, Feddermann N, Ineichen K, Nagaraj VJ, Wiemken A, Boller T, Salzer P. 2005. Ectopic expression of the mycorrhiza-specific chitinase gene *Mtchit 3-3* in *Medicago truncatula* root-organ cultures stimulates spore germination of glomalean fungi. *New Phytologist* **167**: 557–570.

Fahraeus G. 1957. The infection of clover root hairs by nodule bacteria studied by a simple glass slide technique. *Journal of General Microbiology* **16**: 374–381.

Feng F, Sun J, Radhakrishnan GV, Lee T, Bozsoki Z, Fort S, Gavrin A, Gysel K, Thygesen MB, Andersen KR *et al.* 2019. A combination of chitooligosaccharide and lipochitooligosaccharide recognition promotes arbuscular mycorrhizal associations in *Medicago truncatula*. *Nature Communications* **10**: 5047.

Fernández I, Cosme M, Stringlis IA, Yu K, de Jonge R, van Wees SCM, Pozo MJ, Pieterse CMJ, van der Heijden MGA. 2019. Molecular dialogue between arbuscular mycorrhizal fungi and the nonhost plant *Arabidopsis thaliana* switches from initial detection to antagonism. *New Phytologist* **223**: 867–881.

Fiorilli V, Vallino M, Biselli C, Faccio A, Bagnaresi P, Bonfante P. 2015. Host and non-host roots in rice: cellular and molecular approaches reveal differential responses to arbuscular mycorrhizal fungi. *Frontiers in Plant Science* **6**: 636.

Fournier J, Teillet A, Chabaud M, Ivanov S, Genre A, Limpens E, de Carvalho-Niebel F, Barker DG. 2015. Remodeling of the infection chamber before infection thread formation reveals a two-step mechanism for rhizobial entry into the host legume root hair. *Plant Physiology* **167**: 1233–1242.

Gaude N, Bortfeld S, Duensing N, Lohse M, Krajinski F. 2012. Arbuscule-containing and non-colonized cortical cells of mycorrhizal roots undergo extensive and specific reprogramming during arbuscular mycorrhizal development. *The Plant Journal* **69**: 510–528.

Genre A, Chabaud M, Balzergue C, Puech-Pages V, Novero M, Rey T, Fournier J, Rochange S, Becard G, Bonfante P *et al.* 2013. Short-chain chitin oligomers from arbuscular mycorrhizal fungi trigger nuclear Ca^{2+} spiking in *Medicago truncatula* roots and their production is enhanced by strigolactone. *New Phytologist* **198**: 190–202.

Genre A, Russo G. 2016. Does a common pathway transduce symbiotic signals in plant–microbe interactions? *Frontiers in Plant Science* 7: 96.

Gibelin-Viala C, Amblard E, Puech-Pages V, Bonhomme M, Garcia M, Bascaules-Bedin A, Fliegmann J, Wen J, Mysore KS, Signor C *et al.* 2019. The *Medicago truncatula* LysM receptor-like kinase LYK9 plays a dual role in immunity and the arbuscular mycorrhizal symbiosis. *New Phytologist* **223**: 1516–1529.

Giovannetti M, Mosse B. 1980. An evaluation of techniques for measuring vesicular arbuscular mycorrhizal infection in roots. *New Phytologist* **84**: 489–500.

Girardin A, Wang T, Ding Y, Keller J, Buendia L, Gaston M, Ribeyre C, Gasciolli V, Auriac MC, Vernié T *et al.* 2019. LCO receptors involved in arbuscular mycorrhiza are functional for rhizobia perception in legumes. *Current Biology* **29**: 4249–4259.

Gomez SK, Javot H, Deewatthanawong P, Torres-Jerez I, Tang Y, Blancaflor EB, Udvardi MK, Harrison MJ. 2009. *Medicago truncatula* and *Glomus intraradices* gene expression in cortical cells harboring arbuscules in the arbuscular mycorrhizal symbiosis. *BMC Plant Biology* **9**: 10.

Goormachtig S, Lievens S, Van de Velde W, Van Montagu M, Holsters M. 1998. Srchi13, a novel early nodulin from *Sesbania rostrata*, is related to acidic class III chitinases. *Plant Cell* **10**: 905–915.

Gutjahr C, Sawers RJ, Marti G, Andres-Hernandez L, Yang SY, Casieri L, Angliker H, Oakeley EJ, Wolfender JL, Abreu-Goodger C *et al.* 2015. Transcriptome diversity among rice root types during asymbiosis and interaction with arbuscular mycorrhizal fungi. *Proceedings of the National Academy of Sciences, USA* **112**: 6754–6759.

Gutternigg M, Kretschmer-Lubich D, Paschinger K, Rendic D, Hader J, Geier P, Ranftl R, Jantsch V, Lochnit G, Wilson IB. 2007. Biosynthesis of truncated *N*-linked oligosaccharides results from non-orthologous hexosaminidase-mediated mechanisms in nematodes, plants, and insects. *The Journal of Biological Chemistry* **282**: 27825–27840.

He J, Zhang C, Dai H, Liu H, Zhang X, Yang J, Chen X, Zhu Y, Wang D, Qi X *et al.* 2019. A LysM receptor heteromer mediates perception of arbuscular mycorrhizal symbiotic signal in rice. *Molecular Plant* **12**: 1561–1576.

Heidstra R, Geurts R, Franssen H, Spaink HP, Van Kammen A, Bisseling T. 1994. Root hair deformation activity of nodulation factors and their fate on *Vicia sativa*. *Plant Physiology* **105**: 787–797.

Hoffmann B, Trinh TH, Leung J, Kondorosi A, Kondorosi E. 1997. A new *Medicago truncatula* line with superior *in vitro* regeneration, transformation, and symbiotic properties isolated through cell culture selection. *Molecular Plant–Microbe Interactions* **10**: 307–315.

Hood EE, Gelvin SB, Melchers LS, Hoekema A. 1993. New *Agrobacterium* helper plasmids for gene transfer to plants. *Transgenic Research* **2**: 208–218.

Hooykaas MJG, Hooykaas PJJ. 2021. The genome sequence of hairy root *Rhizobium rhizogenes* strain LBA9402: bioinformatics analysis suggests the presence of a new opine system in the agropine Ri plasmid. *MicrobiologyOpen* **10**: e1180.

Hou Y, Vocadlo DJ, Leung A, Withers SG, Mahuran D. 2001. Characterization of the Glu and Asp residues in the active site of human β-hexosaminidase B. *Biochemistry* **40**: 2201–2209.

Jardinaud MF, Boivin S, Rodde N, Catrice O, Kisiala A, Lepage A, Moreau S, Roux B, Cottret L, Sallet E *et al.* 2016. A laser dissection-RNAseq analysis highlights the activation of cytokinin pathways by Nod factors in the *Medicago truncatula* root epidermis. *Plant Physiology* **171**: 2256–2276.

Khokhani D, Carrera Carriel C, Vayla S, Irving TB, Stonoha-Arther C, Keller NP, Ané JM. 2021. Deciphering the chitin code in plant symbiosis, defense, and microbial networks. *Annual Review of Microbiology* **75**: 583–607.

Kobae Y, Kawachi M, Saito K, Kikuchi Y, Ezawa T, Maeshima M, Hata S, Fujiwara T. 2015. Up-regulation of genes involved in *N*-acetylglucosamine uptake and metabolism suggests a recycling mode of chitin in intraradical mycelium of arbuscular mycorrhizal fungi. *Mycorrhiza* **25**: 411–417.

Lefebvre B, Klaus-Heisen D, Pietraszewska-Bogiel A, Herve C, Camut S, Auriac MC, Gasciolli V, Nurisso A, Gadella TW, Cullimore J. 2012. Role of *N*-glycosylation sites and CXC motifs in trafficking of *Medicago truncatula* Nod factor perception protein to plasma membrane. *The Journal of Biological Chemistry* **287**: 10812–10823.

Lever M. 1972. A new reaction for colorimetric determination of carbohydrates. *Analytical Biochemistry* **47**: 273–279.

Lévy J, Bres C, Geurts R, Chalhoub B, Kulikova O, Duc G, Journet EP, Ané J, Lauber E, Bisseling T *et al.* 2004. A putative Ca^{2+} and calmodulin-dependent protein kinase required for bacterial and fungal symbioses. *Science* **303**: 1361–1364.

Li RJ, Zhang CX, Fan SY, Wang YH, Wen J, Mysore KS, Xie ZP, Staehelin C. 2022. The *Medicago truncatula* hydrolase MtCHIT5b degrades Nod factors of *Sinorhizobium meliloti* and cooperates with MtNFH1 to regulate the nodule symbiosis. *Frontiers in Plant Science* **13**: 1034230.

Li SC, Li YT. 1970. Studies on the glycosidases of jack bean meal. *The Journal of Biological Chemistry* **245**: 5153–5160.

Liebminger E, Veit C, Pabst M, Batoux M, Zipfel C, Altmann F, Mach L, Strasser R. 2011. β-*N*-acetylhexosaminidases HEXO1 and HEXO3 are responsible for the formation of paucimannosidic *N*-glycans in *Arabidopsis thaliana*. *The Journal of Biological Chemistry* **286**: 10793–10802.

Liu CW, Breakspear A, Guan D, Cerri MR, Jackson K, Jiang S, Robson F, Radhakrishnan GV, Roy S, Bone C *et al.* 2019. NIN acts as a network hub controlling a growth module required for rhizobial infection. *Plant Physiology* **179**: 1704–1722.

Liu T, Duan Y, Yang Q. 2018. Revisiting glycoside hydrolase family 20 β-*N*-acetyl-D-hexosaminidases: crystal structures, physiological substrates and specific inhibitors. *Biotechnology Advances* **36**: 1127–1138.

Liu Y, Yu SX, Xie ZP, Staehelin C. 2012. Analysis of a negative plant–soil feedback in a subtropical monsoon forest. *Journal of Ecology* **100**: 1019–1028.

Luginbuehl LH, Menard GN, Kurup S, Van Erp H, Radhakrishnan GV, Breakspear A, Oldroyd GED, Eastmond PJ. 2017. Fatty acids in arbuscular mycorrhizal fungi are synthesized by the host plant. *Science* **356**: 1175–1178.

Maillet F, Poinsot V, André O, Puech-Pagès V, Haouy A, Gueunier M, Cromer L, Giraudet D, Formey D, Niebel A *et al.* 2011. Fungal lipochitooligosaccharide symbiotic signals in arbuscular mycorrhiza. *Nature* **469**: 58–63.

Malolepszy A, Kelly S, Sorensen KK, James EK, Kalisch C, Bozsoki Z, Panting M, Andersen SU, Sato S, Tao K *et al.* 2018. A plant chitinase controls cortical infection thread progression and nitrogen-fixing symbiosis. *eLife* **7**: e38874.

Mitra RM, Gleason CA, Edwards A, Hadfield J, Downie JA, Oldroyd GE, Long SR. 2004. A Ca^{2+}/calmodulin-dependent protein kinase required for symbiotic nodule development: gene identification by transcript-based cloning. *Proceedings of the National Academy of Sciences, USA* **101**: 4701–4705.

Nadal M, Sawers R, Naseem S, Bassin B, Kulicke C, Sharman A, An G, An K, Ahern KR, Romag A *et al.* 2017. An *N*-acetylglucosamine transporter required for arbuscular mycorrhizal symbioses in rice and maize. *Nature Plants* **3**: 17073.

Ovtsyna AO, Schultze M, Tikhonovich IA, Spaink HP, Kondorosi E, Kondorosi A, Staehelin C. 2000. Nod factors of *Rhizobium leguminosarum* bv. *viciae* and their fucosylated derivatives stimulate a Nod factor cleaving activity in pea roots and are hydrolyzed *in vitro* by plant chitinases at different rates. *Molecular Plant–Microbe Interactions* **13**: 799–807.

Paszkowski U, Jakovleva L, Boller T. 2006. Maize mutants affected at distinct stages of the arbuscular mycorrhizal symbiosis. *The Plant Journal* **47**: 165–173.

Perret X, Staehelin C, Broughton WJ. 2000. Molecular basis of symbiotic promiscuity. *Microbiology and Molecular Biology Reviews* **64**: 180–201.

Pislariu CI, Murray JD, Wen J, Cosson V, Muni RR, Wang M, Benedito VA, Andriankaja A, Cheng X, Jerez IT *et al.* 2012. A *Medicago truncatula* tobacco retrotransposon insertion mutant collection with defects in nodule development and symbiotic nitrogen fixation. *Plant Physiology* **159**: 1686–1699.

Price NP, Relić B, Talmont F, Lewin A, Promé D, Pueppke SG, Maillet F, Dénarié J, Promé JC, Broughton WJ. 1992. Broad-host-range *Rhizobium* species strain NGR234 secretes a family of carbamoylated, and fucosylated, nodulation signals that are *O*-acetylated or sulphated. *Molecular Microbiology* **6**: 3575–3584.

Pueppke SG, Broughton WJ. 1999. *Rhizobium* sp. NGR234 and *R. fredii* USDA257 share exceptionally broad, nested host ranges. *Molecular Plant–Microbe Interactions* **12**: 293–318.

Radutoiu S, Madsen LH, Madsen EB, Jurkiewicz A, Fukai E, Quistgaard EM, Albrektsen AS, James EK, Thirup S, Stougaard J. 2007. LysM domains mediate lipochitin-oligosaccharide recognition and *Nfr* genes extend the symbiotic host range. *EMBO Journal* **26**: 3923–3935.

Rasmussen SR, Füchtbauer W, Novero M, Volpe V, Malkov N, Genre A, Bonfante P, Stougaard J, Radutoiu S. 2016. Intraradical colonization by arbuscular mycorrhizal fungi triggers induction of a lipochitooligosaccharide receptor. *Scientific Reports* **6**: 29733.

Reissig JL, Strominger JL, Leloir LF. 1955. A modified colorimetric method for the estimation of *N*-acetylamino sugars. *The Journal of Biological Chemistry* **217**: 959–966.

Roy S, Liu W, Nandety RS, Crook A, Mysore KS, Pislariu CI, Frugoli J, Dickstein R, Udvardi MK. 2020. Celebrating 20 years of genetic discoveries in legume nodulation and symbiotic nitrogen fixation. *Plant Cell* **32**: 15–41.

Rush TA, Puech-Pages V, Bascaules A, Jargeat P, Maillet F, Haouy A, Maes AQ, Carriel CC, Khokhani D, Keller-Pearson M *et al.* 2020. Lipo-chitooligosaccharides as regulatory signals of fungal growth and development. *Nature Communications* **11**: 3897.

Sagan M, deLarambergue H, Morandi D. 1998. Genetic analysis of symbiosis mutants in *Medicago truncatula*. In: Elmerich C, Kondorosi A, Newton WE, eds. *Biological nitrogen fixation for the 21st century*. Dordrecht, the Netherlands: Kluwer Academic, 317–318.

Schiessl K, Lilley JLS, Lee T, Tamvakis I, Kohlen W, Bailey PC, Thomas A, Luptak J, Ramakrishnan K, Carpenter MD *et al.* 2019. *NODULE INCEPTION* recruits the lateral root developmental program for symbiotic nodule organogenesis in *Medicago truncatula*. *Current Biology* **29**: 3657–3668.

Schultze M, Quiclet-Sire B, Kondorosi E, Virelizer H, Glushka JN, Endre G, Géro SD, Kondorosi A. 1992. *Rhizobium meliloti* produces a family of sulfated lipooligosaccharides exhibiting different degrees of plant host specificity. *Proceedings of the National Academy of Sciences, USA* **89**: 192–196.

Schultze M, Staehelin C, Brunner F, Genetet I, Legrand M, Fritig B, Kondorosi E, Kondorosi A. 1998. Plant chitinase/lysozyme isoforms show distinct substrate specificity and cleavage site preference towards lipochitooligosaccharide Nod signals. *The Plant Journal* **16**: 571–580.

Smith SE, Read D. 2008. *Mycorrhizal symbiosis*. Cambridge, UK: Academic Press.

Spaink HP, Sheeley DM, van Brussel AA, Glushka J, York WS, Tak T, Geiger O, Kennedy EP, Reinhold VN, Lugtenberg BJ. 1991. A novel highly unsaturated fatty acid moiety of lipo-oligosaccharide signals determines host specificity of *Rhizobium*. *Nature* **354**: 125–130.

Staehelin C, Granado J, Müller J, Wiemken A, Mellor RB, Felix G, Regenass M, Broughton WJ, Boller T. 1994a. Perception of *Rhizobium* nodulation factors by tomato cells and inactivation by root chitinases. *Proceedings of the National Academy of Sciences, USA* **91**: 2196–2200.

Staehelin C, Schultze M, Kondorosi E, Mellor RB, Boller T, Kondorosi A. 1994b. Structural modifications in *Rhizobium meliloti* Nod factors influence their stability against hydrolysis by root chitinases. *The Plant Journal* **5**: 319–330.

Staehelin C, Xie ZP, Illana A, Vierheilig H. 2011. Long-distance transport of signals during symbiosis: are nodule formation and mycorrhization autoregulated in a similar way? *Plant Signaling & Behavior* **6**: 372–377.

Strasser R, Bondili JS, Schoberer J, Svoboda B, Liebminger E, Glössl J, Altmann F, Steinkellner H, Mach L. 2007. Enzymatic properties and subcellular localization of *Arabidopsis* β-*N*-acetylhexosaminidases. *Plant Physiology* **145**: 5–16.

Sun J, Miller JB, Granqvist E, Wiley-Kalil A, Gobbato E, Maillet F, Cottaz S, Samain E, Venkateshwaran M, Fort S *et al.* 2015. Activation of symbiosis signaling by arbuscular mycorrhizal fungi in legumes and rice. *Plant Cell* **27**: 823–838.

Tadege M, Wen J, He J, Tu H, Kwak Y, Eschstruth A, Cayrel A, Endre G, Zhao PX, Chabaud M *et al.* 2008. Large-scale insertional mutagenesis using the *Tnt1* retrotransposon in the model legume *Medicago truncatula*. *The Plant Journal* **54**: 335–347.

Tian Y, Liu W, Cai J, Zhang LY, Wong KB, Feddermann N, Boller T, Xie ZP, Staehelin C. 2013. The nodulation factor hydrolase of *Medicago truncatula*: characterization of an enzyme specifically cleaving rhizobial nodulation signals. *Plant Physiology* **163**: 1179–1190.

Tominaga T, Yao L, Saito H, Kaminaka H. 2022. Conserved and diverse transcriptional reprogramming triggered by the establishment of symbioses in tomato roots forming *Arum*-type and *Paris*-type arbuscular mycorrhizae. *Plants* **11**: 747.

Trinh TH, Ratet P, Kondorosi E, Durand P, Kamaté K, Bauer P, Kondorosi A. 1998. Rapid and efficient transformation of diploid *Medicago truncatula* and *Medicago sativa* ssp. *falcata* lines improved in somatic embryogenesis. *Plant Cell Reports* **17**: 345–355.

Tsujimori Y, Ogura M, Rahman MZ, Maeda M, Kimura Y. 2019. Plant complex type free *N*-glycans occur in tomato xylem sap. *Bioscience Biotechnology Biochemistry* **83**: 1310–1314.

Van Brussel AAN, Tak T, Wetselaar A, Pees E, Wijffelman C. 1982. Small leguminosae as test plants for nodulation of *Rhizobium leguminosarum* and other rhizobia and agrobacteria harbouring a leguminosarum sym-plasmid. *Plant Science Letters* **27**: 317–325.

Vierheilig H, Coughlan AP, Wyss U, Piche Y. 1998. Ink and vinegar, a simple staining technique for arbuscular-mycorrhizal fungi. *Applied and Environmental Microbiology* **64**: 5004–5007.

Volpe V, Chialva M, Mazzarella T, Crosino A, Capitanio S, Costamagna L, Kohlen W, Genre A. 2023. Long-lasting impact of chitooligosaccharide application on strigolactone biosynthesis and fungal accommodation promotes arbuscular mycorrhiza in *Medicago truncatula*. *New Phytologist* **237**: 2316–2331.

Walker L, Lagunas B, Gifford ML. 2020. Determinants of host range specificity in legume-rhizobia symbiosis. *Frontiers in Microbiology* **11**: 585749.

Wang D, Dong W, Murray J, Wang E. 2022. Innovation and appropriation in mycorrhizal and rhizobial symbioses. *Plant Cell* **34**: 1573–1599.

Yang J, Lan L, Jin Y, Yu N, Wang D, Wang E. 2022. Mechanisms underlying legume-rhizobium symbioses. *Journal of Integrative Plant Biology* **64**: 244–267.

Zeng T, Holmer R, Hontelez J, Te Lintel-Hekkert B, Marufu L, de Zeeuw T, Wu F, Schijlen E, Bisseling T, Limpens E. 2018. Host- and stage-dependent

secretome of the arbuscular mycorrhizal fungus *Rhizophagus irregularis*. *The Plant Journal* **94**: 411–425.

Zeng T, Rodriguez-Moreno L, Mansurkhodzaev A, Wang P, van den Berg W, Gasciolli V, Cottaz S, Fort S, Thomma B, Bono JJ *et al.* 2020. A lysin motif effector subverts chitin-triggered immunity to facilitate arbuscular mycorrhizal symbiosis. *New Phytologist* **225**: 448–460.

Zeng Z, Liu Y, Feng XY, Li SX, Jiang XM, Chen JQ, Shao ZQ. 2023. The RNAome landscape of tomato during arbuscular mycorrhizal symbiosis reveals an evolving RNA layer symbiotic regulatory network. *Plant Communications* **4**: 100429.

Zhang C, He J, Dai H, Wang G, Zhang X, Wang C, Shi J, Chen X, Wang D, Wang E. 2021. Discriminating symbiosis and immunity signals by receptor competition in rice. *Proceedings of the National Academy of Sciences, USA* **118**: e2023738118.

Supporting Information

Additional Supporting Information may be found online in the Supporting Information section at the end of the article.

Fig. S1 Expression data of GH20 genes obtained from the *Medicago truncatula* Gene Expression Atlas.

Fig. S2 Expression data of GH20 genes in *M. truncatula* obtained from the Symbimics database.

Fig. S3 Amino acid sequence alignment of GH20 proteins deduced from nucleotide sequences of *A. thaliana* and *M. truncatula*.

Fig. S4 Phylogenetic analysis of plant GH20 protein sequences.

Fig. S5 Exon–intron architecture of GH20 genes in *A. thaliana* and *M. truncatula*.

Fig. S6 Spot inoculation experiment with *F. oxysporum*.

Fig. S7 Alignment of *MtHEXO2* promoter sequences in *M. truncatula* Jemalong A17 and R108 genomes.

Fig. S8 qRT-PCR analysis of *MtHEXO2* transcripts in roots of Jemalong A17 wild-type (WT), *dmi3-1*, and *dmi1-3* mutant plants.

Fig. S9 Alignment of *MtHEXO2* nucleotide sequences obtained from *M. truncatula* Jemalong A17 and R108.

Fig. S10 Alignment of MtHEXO2 protein sequences from *M. truncatula* Jemalong A17 and R108.

Fig. S11 Expression of His-tagged MtHEXO2 and the D325A/E326A variant in *E. coli* BL21 (DE3).

Fig. S12 Preparation of a polyclonal rabbit serum against MtHEXO2.

Fig. S13 His-tagged MtHEXO2 expressed in *E. coli* BL21 (DE3) hydrolyzes *p*NP-GlcNAc.

Fig. S14 Hydrolysis of chitohexaose and chitoheptaose by MtHEXO2 expressed in *P. pastoris*.

Fig. S15 Recombinant MtHEXO2 secreted by *P. pastoris* did not cleave NodSm-IV(C16:2, S).

Fig. S16 Recombinant MtHEXO2 secreted by *P. pastoris* did not cleave LCOs from *Sinorhizobium* sp. NGR234.

Fig. S17 Analysis of *hexo2* mutants by PCR.

Fig. S18 qRT-PCR analysis of plant defense-related marker genes in roots of *M. truncatula* wild-type (WT) and *hexo2* mutant plants inoculated with *R. intraradices* (AM) or mock-inoculated with sterilized substrate (Mock).

Fig. S19 *M. truncatula* plants constitutively overexpressing *MtHEXO2* did not show altered colonization by *R. intraradices*.

Fig. S20 *MtHEXO2* expression analysis by reverse transcription PCR in complementation experiments.

Fig. S21 Degree of root colonization by *R. intraradices* in *M. truncatula* plants treated with or without GlcNAc.

Methods S1 Purification of His-tagged MtHEXO2 expressed in *E. coli*.

Methods S2 Preparation of recombinant MtHEXO2 expressed in *P. pastoris*.

Methods S3 Protein analysis and Western blots.

Methods S4 Purification and quantification of LCOs from *Sinorhizobium* sp. NGR234.

Methods S5 Preparation of sulfated chitobiose.

Methods S6 Treatment of *M. truncatula* with COs, NodSm-IV (C16:2, S), and LCOs from *Sinorhizobium* sp. NGR234.

Methods S7 Enzyme assays with aryl glycosides.

Methods S8 Quantification of GlcNAc enzymatically released from COs.

Methods S9 HPLC analysis of GlcNAc and COs obtained from hydrolysis of chitopentaose by recombinant MtHEXO2.

Methods S10 Analysis of sulfated chitobiose and chitobiose by thin-layer chromatography.

Methods S11 NodSm-IV(C16:2, S) hydrolysis assay.

Methods S12 Hydrolysis assay of LCOs from *Sinorhizobium* sp. NGR234.

Methods S13 Seed germination.

Methods S14 Inoculation of *M. truncatula* with AM fungi.

Methods S15 Inoculation of *M. truncatula* with *S. meliloti*.

Methods S16 Visualization of AM structures with Alexa Fluor 488.

Methods S17 Microscopic protein localization analysis.

Methods S18 Hairy root transformation.

Methods S19 Construction of *M. truncatula* plants constitutively overexpressing *MtHEXO2*.

Methods S20 Histochemical GUS staining and sectioning of nodules.

Table S1 Strains and plasmids used in this study.

Table S2 Primers used in this study.

Table S3 Nodule number of *M. truncatula* wild-type (WT) and *hexo2* mutant plants (numerical data).

Table S4 Root colonization by *R. intraradices* in *M. truncatula* wild-type (WT) and *hexo2* mutant plants (numerical data).

Table S5 Root colonization by *R. intraradices* in *M. truncatula* wild-type (WT), constitutively overexpressing *MtHEXO2* (OE) and *hexo2-1* mutant plants (numerical data).

Table S6 Hairy root transformation efficiency of *hexo2* mutants in complementation experiments.

Table S7 Root colonization by *R. intraradices* in complementation experiments with *hexo2* mutant plants (numerical data).

Please note: Wiley is not responsible for the content or functionality of any Supporting Information supplied by the authors. Any queries (other than missing material) should be directed to the *New Phytologist* Central Office.